Antifungal effects of ZnO, TiO_2 and ZnO-TiO_2 nanocomposite on *Aspergillus flavus*

nasrollah najibi ilkhechi (nasrollah.najibi@gmail.com)
Sahand University of Technology
Mahdi Mozammel
sahand university of technology
Ahmad Yari Khoroushahi
Tabriz University of Medical Sciences

Research Article

Keywords: Aspergillus flavus, antifungal, ROS, ZnO-TiO2, Sol-gel

Posted Date: December 10th, 2020

DOI: https://doi.org/10.21203/rs.3.rs-123795/v1

Abstract

This study aimed to synthesis ZnO, TiO_2 and ZnO–TiO_2 (ratio weight of 1/1 for Zn/Ti) nanoparticles using zinc acetate and titanium isopropoxide through the sol-gel method. Physicochemical and morphological characterization and antifungal properties evaluation like minimum inhibition concentration (MIC) and minimum fungicide concentration (MFC) of nanopowders were investigated against *Aspergillus flavus* at *in vitro*. All synthesized nanoparticles (50 µg/ml) showed fungal growth inhibition while ZnO-TiO_2 showed higher antifungal activity against *A. flavus* than pure TiO_2 and ZnO. TiO_2 and ZnO-TiO_2 (300 µg/ml) inhibited 100% of spur production. Pure ZnO and TiO_2 showed pyramidal and spherical shapes, respectively whereas ZnO-TiO_2 nanopowders illustrated both spherical and pyramidal shapes with grown particles on the surface. Based on our findings, low concentration (150 µg/ml) of ZnO-TiO_2 showed higher ROS production and stress oxidative induction thus fungicide effect as compared to alone TiO_2 and ZnO. In conclusion, ZnO-TiO_2 nanostructure can be utilized as an effective antifungal compound but more studies need to be performed to understand the antifungal mechanism of the nanoparticles rather than ROS inducing apoptosis.

1. Introduction

ZnO and TiO_2 have been used in various biomedical applications due to photocatalytic, antimicrobial and antifungal properties [1, 2]. Doping and nanocomposite manufacturing have been previously utilized as the processes for enhancing the antifungal activity of this kind of nanoparticles. Among the various semiconductor nanomaterials, titanium dioxide (TiO_2) and zinc oxide (ZnO) have achieved more attention due to their high chemical stability, nontoxicity, relatively low cost and high antimicrobial activity [3, 4]. The metal oxide NPs antibacterial and antifungal properties have been previously studied [5–7] and the findings showed the ZnO antibacterial activity as well its capability to increase of induction of reactive oxygen species (ROS) production by decreasing its particle size. The zinc oxide antifungal activity is related to the formation of free radicals on the surface of nanoparticles that damage the fungal cell membrane lipids, which lead to protein leakage through the membrane disruption [8–12].

TiO_2 NPs possess the antimicrobial properties even at low concentrations through the photocatalytic process that causes fatal damage in treated microorganisms [13–15]. Based on TiO_2 nanoparticle antimicrobial properties, these nanoparticles in the anatase and rutile phase show the excellent antifungal properties [16]. The titania owned enormous applications because of its high thermal/chemical stability, and high photocatalytic activity. The toxicity of titania nanoparticles originates from its physical properties, not its chemical structure. These nanoparticles can permeate from biological barriers that can damage the cells or even organs. Some methodologies have been previously applied for improving the titania NPs' antimicrobial activities on simple microorganisms such as bacteria and viruses [17–21].

By considering the *Aspergillus* species as the deadliest opportunistic fungal infections, these fungi are the main threat to human health. Among the 600 species of *Aspergillus*, the *flavus*, *fumigatus*, and *niger* species possess the pathogenicity for humans and growing on crops can cause the occurrence of some disease [22, 23]. Upon the previous quantitative reports on ZnO and TiO2 fungal growth inhibition, these nanoparticles possess fungicidal effects on *Candida albicans*, *Aspergillus niger*, and *Penicillium* sp. fungus. We showed previously the increase of ZnO and TiO_2 antibacterial activity by increasing the concentration of dopant in doped ZnO and TiO_2 [24, 25]. This study aimed to synthesize the ZnO, TiO_2, and ZnO-TiO_2 nanostructures using the sol-gel methodology, physicochemical characterization of nanopowders, and antifungal assays against *Aspergillus flavus* to find the highly effective antifungal concentration at dark condition.

2. Experimental

2.1. Nanostructures synthesis

ZnO and TiO_2 nanostructures were synthesized using the sol-gel method as described by Najibi [25]. For the preparation of ZnO-TiO_2 nanostructures, separately prepared ZnO and TiO_2 sols were mixed at the same molar ratio of Zn:Ti then the mixture was stirred at ambient temperature for 2 h and the stirred solution was remained for 24 h to obtain a gel. Prepared gel was dried at 100 °C and was calcined at 500 °C for 2.5 hours.

2.2. Material characterization method

The XRD pattern and phase identification of nanopowders were determined by X-RAY diffraction analysis (Philips-MPD XPERT, λ: CuKᾱ=0.154 nm) and 20–70˚ range of scanned samples were considered as 2Θ. The scanning electron microscopy (SEM), transmission electron microscopy (TEM), particle size analyzer (N5, Backman, USA), and zeta potential analyzer (Malvern Zeta- sizer 3000, Malvern Instrument Inc., London, UK) were utilized for morphological, size, and zeta potential characterization of all samples, respectively. Fourier Transform Infrared (FTIR) Spectroscopy was used to identify organic, polymeric, and in some cases, inorganic materials. Fourier transforms infrared (FTIR) spectra were obtained using a Bruker IFS 48 instrument (Bruker Optik GmbH, Germany). All spectra were taken under air as a function of time with 16 scans at a resolution of 4 cm^{-1} and a spectral range of 4000–5000 cm^{-1}.

2.3. Antifungal assay

A. flavus, purchased from the Iranian biological resource center (IBRC), were cultured on Sabouraud dextrose agar (SDA; Merck, Darmstadt, Germany) at 25 °C and the dark condition. The autoclaved SDA media containing ZnO, TiO_2 and ZnO-TiO_2 NPs at concentrations of 0, 37, 75,150 and 300 μg $ml^{-1}$and an NP-free solution were poured onto the 6 cm diameter Petri dishes. To determination of minimum inhibition concentration (MIC) of nanoparticles for each treatment group, the CLSI-M38 standard method was used for the time intervals of 7 days by measuring the diameter of fungal colonies opacity. To

determine the minimum fungicide concentration (MFC), the higher concentrations than MIC for each nanostructure were used on SDA medium similar to the MIC determination experiment and the minimum concentration that killed *A. flavus* considered as MFC. To detect the production of ROS after each time point of treatment, 2'-7'-Dichlorodihydrofluorescein diacetate (DCFH-DA) solubilized in ethanol (5 µM final concentration) was added to the cultures and incubated on a shaker at room temperature at the dark condition for 1 h. DCFH-DA, a nonpolar dye, is converted to the nonfluorescent polar derivative DCFH by cellular esterases. DCFH can switch to highly fluorescent DCF through oxidization by intracellular ROS and possessing an excitation wavelength of 485 nm and an emission band between 500 and 600 nm. After incubation time, samples were subjected to fluorescence microscopy (Biozero BZ-8000; Keyence, Osaka, Japan) equipped with the following filter set EX 495 nm EM 510 nm, and fluorescence spectrophotometric (RF-5000, Shimadzu, Kyoto, Japan) analysis at room temperature.

3. Results And Discussions

3.1 XRD and phase structure of nanostructures

ZnO and TiO_2 showed the crystalline nature with wurtzite and anatase structure, respectively. The crystalline ZnO illustrated the diffraction peaks at 2θ = 36.02°, 31.7°, 34.3°, 47.5°, 56.5°, 62.8°, 66.3°, and 67.8. the anatase phases of TiO_2 indicated peaks at 2θ = 25.4°, 38.1°, 48.1°, 54.8°, 62.5°, and 75.1° [26]. The XRD patterns of ZnO and TiO_2 showed a single high-intensity peak that implies a highly oriented and single-crystalline nature of the samples. As shown in Fig. 1, the intensity of TiO_2 peaks considerably decreased after the addition of TiO_2 into the structure of ZnO in the ZnO-TiO_2 composite that indicates the greater crystallinity of pure TiO_2NPs compared to ZnO-TiO_2 NPs [27]. Profile broadening also indicated the small crystalline domain sizes of wurtzite and anatase indicating that the ZnO-TiO_2 composite hinders the growth of particles during calcination. The main peaks of each sample in the range of $2\theta = 20–50°$ specified some peaks belonging to anatase (Fig. 1).

Table 1 demonstrated the variations of the crystallite size, surface area, the lattice constant *a* and the lattice constant *c* for ZnO, TiO_2 and ZnO-TiO_2 composite. The crystallite size of the pure ZnO and TiO_2 was 33.21 and 17.68 nm, respectively. The ZnO-TiO_2 composite nanoparticles showed the lower particle size compared to each ZnO and TiO_2 alone nanoparticles.

Table 1
Characterization of ZnO,TiO_2 and ZnO-TiO_2

Sample	Crystallite size(nm)	a = b(Å)	c(Å)	S m^2/g	PSA(nm)	Zeta Potential(mv)	MIC (µg/ml)	MFC (µg/ml)
ZnO	33.21	3.242	5.214	32.20	608	-11.6	156	312
TiO_2	17.68	3.798	8.944	98.36	299	-36.4	78	156
ZnO-TiO_2	ZnO = 19.25 TiO_2 = 8.36	3.253 3.807	5.238 9.592	131.78	983	-12	39	78

By considering the lattice constant and surface area data in Table 1, the significant increase of specific area from 32.20 to 131.78 m^2/g of ZnO-TiO_2 was observed compared to the pure ZnO and TiO_2 by increasing crystallite size. The increase in the value of lattice parameters for ZnO-TiO_2 can be attributed to the incorporation of ions (Ti^{+4} and Zn^{+2}), which is due to stress in crystal structures.

3.2 PSA and Zeta potential analysis

The zeta potential is an important indicator of the stability of dispersed particles in the suspension solution. The zeta potential determines the repulsion of dispersed particles in the solution. Small particles require the high zeta potential for superior stability, and low zeta potential causes to particle accumulation. The zeta potential of a particle alters by the particle surface chemical composition, the pH and ionic strength of the solution. Zeta potential of ZnO, TiO_2, and ZnO-TiO_2 were − 11.6, -36.4, and − 12 mV, respectively (Fig. 2 and Table 1). Based on our findings, TiO_2 and ZnO-TiO_2 showed the highest and lowest stability in aqueous suspension, respectively. Larger particle sizes for ZnO (608 nm), TiO2 (299 nm), and ZnO-TiO2 (983 nm) were determined by PSA analysis showing the agglomeration of nanoparticles.

3.4 SEM and TEM analysis

As shown in Fig. 3, the ZnO and TiO_2 nanoparticles illustrated hexagonal-pyramidal and spherical shape with grown articles on surfaces, respectively. The wurtzite-structured ZnOcrystal is described as several alternating planes composed of four-fold tetrahedrally-coordinated $O^{2-}$and Zn^{2+} ions stacked alternatively along the c-axis [28]. The oppositely-charged ions produce positively-charged Zn (0001) and negatively-charged O(0001$^-$) surfaces, resulting in a normal dipole moment and spontaneous polarization along the c-axis, as well as a divergence.

In the ZnO-TiO_2 nanostructures, the morphology was a mixture of pyramidal and spherical with more agglomeration while the particle sizes were smaller than alone titanium and zinc oxide particles. Upon the

EDX analysis, the strong signals of Zn, Ti and Zn-Ti were observed in ZnO, TiO_2, and ZnO-TiO_2 nanostructures, respectively (Fig. 3).

The TEM images of nanostructures clarified the regular growth of all nanostructures and illuminated the TiO_2 (5 nm) particle size smaller than ZnO (10 nm) and ZnO-TiO_2 (35 nm) nanoparticles with lower agglomeration rate (Fig. 3).

3.5 FTIR analysis

FTIR was applied to study the component and composite structures of synthesized nanoparticles. Zn-O and Zn-OH bands were observed between 1000 cm^{-1} and 400 cm^{-1} while Ti-O and Ti-OH bands appeared around 480 cm^{-1} and 790 cm^{-1}. The peaks at 672 cm^{-1} and 829 cm^{-1} showed the stretching band of O-Ti-O and Zn-O-Ti vibration mode in TiO_2 (T) and ZnO-TiO_2 (ZT) nanostructures [29, 30]. The peaks in the around of 2800 cm^{-1} and 2900 cm^{-1} were related to the tensile vibrations of CH_3 and CH_2, and the peaks in the range of 1380 cm^{-1} and 1500 cm^{-1} corresponded to the bending vibrations of molecules CH_2 and CH_3, respectively. The broad peak in the range of 3400 cm^{-1} and 3800 cm^{-1} was related to the hydroxyl groups. Also, water molecules in the bending band at 1630 cm^{-1} are visible [31]. The presence of some bands can be associated with the organic phase of solid, despite the use of organic compounds in the synthesis of nanoparticles (Fig. 4).

3.6 Antifungal properties of nanostructures

As shown in Table 1, ZnO-TiO_2 nanostructure exhibits better antifungal effects against *A. flavus* than other nanoparticles due to its high specific surface area. By increasing the specific surface area, the possibility of chemical reactions and the production of reactive oxygen species on the surface were increased [32]. The MIC for ZnO-TiO_2, ZnO, and TiO_2 against *A. flavus* was determined 39, 156, and 78 µg/ml, respectively. Because of the small particle size, the best cell internalization, and the ability to produce more reactive oxygen species, TiO_2 showed a higher fungicide than ZnO. The MFC for ZnO, TiO_2, and ZnO-TiO_2 was 312, 156 and 78 µg/ml, respectively. The particle size of the ZnO-TiO_2 nanostructure possessed a sharp structure with smaller particles than the cell membrane that can inhibit the growth of the fungus by entering the cell membrane and injuring the cell wall thus resulting in the high toxicity. Figure 5 illustrated the inhibition zone of ZnO, TiO_2, and ZnO-TiO_2 at 37.5, 75, 150, and 300 µg/ml concentrations. By increasing the concentration of nanoparticles, inhibition zone diameter of growth increased and 100% of inhibition was achieved at 300 µg/ml for TiO_2 and ZnO-TiO_2 treated groups. The minimum fungal growth (72%) was obtained at 37.5 µg/ml for ZnO-TiO_2 while for ZnO was 50% at the same concentration showing that the TiO_2 synergistic effect into the mixture [33]. Among all nanoparticles, ZnO nanoparticles showed the lowest fungicide activity compared to others whereas it significantly increased the antifungal activity in ZnO-TiO_2 nanocomposite.

The destructive changes were observed on the shape and growth of the treated *A. flavus* (at a concentration of 37.5 µg/ml for all samples) compared to the untreated control group. As shown in Fig. 6, the untreated control fungus produced the highest count of fungal spores while treated groups showed a lower count of spores and damaged tubular filaments, in instance deformation, smoothness, and noticeably thinner in hyphae compared to the untreated group. Upon the previous reports, increasing the hyphae causes to form whiter medium [34] and our findings agreed to color changes based on the used nanoparticles (Fig. 6).

Among the reactive oxygen species, hydrogen peroxide and hydroxyl radicals as the strong and non-selective ROSs can damage all types of biomolecules including carbohydrates, acids, lipids, proteins, DNA, RNA, and amino acids through inducing the oxidative stress [35]. The production rate of the three major reactive oxygen species by ZnO and TiO_2 nanoparticles were: ZnO: $O_2^{\bullet-}$>O_2>$^{\bullet}OH$ and TiO_2: O_2>$^{\bullet}OH$ > $O_2^{\bullet-}$ [36]. There is a direct dependency between increasing the formation of ROS and the fungicide of nanoparticles. As shown in Fig. 7, all nanoparticles raised the ROS production in treated *A. flavus* compared to untreated control with order ZnO-TiO_2 > TiO_2 > ZnO > untreated control. The production of intracellular ROS was influenced by the type and specific surface of nanoparticles. Titania can produce ROS higher than zinc oxide [37], our findings also confirmed the highest ROS production through stronger fluorescence intensity in ZnO-TiO_2 treated group. In ZnO-TiO_2 nanostructures, the specific surface area is higher than other nanoparticles (TiO_2 and ZnO) and accordingly high ROS generation. Oxidative stress induced by reactive oxygen species generation in ZnO-TiO_2 nanostructures is thought to be the main mechanism of antifungal activity. The suggested mechanism for the antifungal activity of these compounds can be based on the formation of high levels of reactive oxygen species (ROS) that disrupt the integrity of the fungal cell membrane, which assists in the damage of microbial enzyme bodies thus killing the fungi [38].

4. Conclusion

This study aimed to compare the antifungal properties of TiO_2 and ZnO versus ZnO-TiO_2 nanocomposites to select the compound with the highest antifungal activity. Based on our findings, low concentration (150 µg/ml) of ZnO-TiO_2 showed higher fungicide and stress oxidative induction through ROS production as compared to TiO_2 and ZnO. In conclusion, ZnO-TiO_2 nanostructure composition can be used as an effective antifungal compound but more studies need to be performed to deeply understand the antifungal mechanism of the nanoparticles rather than stress oxidative induction.

Declarations

Contributions

NNI carried out most of the experiments and wrote this paper. MM participated in this project and proposed the idea. AYKH designed and supported the project edited and revised the paper. All authors

read and approved the final manuscript.

Ethics declarations

Ethics approval and consent to participate

Not applicable.

Consent for publication

Not applicable.

Competing interests

The authors declare no conflict of interest.

References

1. Janitabar-Darzi S, Mahjoub AR, Compounds: Investigation of phase transformations and photocatalytic properties of sol–gel prepared nanostructured ZnO/TiO2 composites. *Journal of Alloys* 2009; 486:805-808.
2. Wahab R, Mishra A, Yun SI, Kim YS, Shin HS: Antibacterial activity of ZnO nanoparticles prepared via non-hydrolytic solution route. *Appl Microbiol Biotechnol* 2010; 87:1917-1925.
3. Sirelkhatim A, Mahmud S, Seeni A, Kaus NHM, Ann LC, Bakhori SKM, Hasan H, Mohamad D: Review on Zinc Oxide Nanoparticles: Antibacterial Activity and Toxicity Mechanism. *Nanomicro Lett* 2015; 7:219-242.
4. Dhobale S, Thite T, Laware S, Rode C, Koppikar SJ, Ghanekar R-K, Kale S: Zinc oxide nanoparticles as novel alpha-amylase inhibitors. *J Journal of Applied Physics* 2008; 104:094907.
5. Zhang Y, Ram MK, Stefanakos EK, Goswami DY: Synthesis, characterization, and applications of ZnO nanowires. *Journal of Nanomaterials* 2012; 2012.
6. Sawai J, Yoshikawa T: Quantitative evaluation of antifungal activity of metallic oxide powders (MgO, CaO and ZnO) by an indirect conductimetric assay. *J Appl Microbiol* 2004; 96:803-809.
7. Sharma D, Rajput J, Kaith B, Kaur M, Sharma S: Synthesis of ZnO nanoparticles and study of their antibacterial and antifungal properties. *Thin solid films* 2010; 519:1224-1229.
8. Lipovsky A, Nitzan Y, Gedanken A, Lubart R: Antifungal activity of ZnO nanoparticles—the role of ROS mediated cell injury. *Nanotechnology* 2011; 22:105101.
9. Perelshtein I, Ruderman E, Perkas N, Tzanov T, Beddow J, Joyce E, Mason TJ, Blanes M, Mollá K, Patlolla A: Chitosan and chitosan–ZnO-based complex nanoparticles: formation, characterization, and antibacterial activity. *Journal of Materials Chemistry B* 2013; 1:1968-1976.
10. Jasim NO: Antifungal activity of Zinc oxide nanoparticles on Aspergillus fumigatus fungus & Candida albicans yeast. *J Nat Sci Res* 2015; 5:23-27.

11. Applerot G, Lipovsky A, Dror R, Perkas N, Nitzan Y, Lubart R, Gedanken A: Enhanced antibacterial activity of nanocrystalline ZnO due to increased ROS-mediated cell injury. *J Advanced Functional Materials* 2009; 19:842-852.
12. Zhang H, Chen G: Potent antibacterial activities of Ag/TiO2 nanocomposite powders synthesized by a one-pot sol-gel method. *Environ Sci Technol* 2009; 43:2905-2910.
13. McCullagh C, Robertson JM, Bahnemann DW, Robertson PK: The application of TiO 2 photocatalysis for disinfection of water contaminated with pathogenic micro-organisms: a review. *Research on Chemical Intermediates* 2007; 33:359-375.
14. Sawai J, Shoji S, Igarashi H, Hashimoto A, Kokugan T, Shimizu M, Kojima H: Hydrogen peroxide as an antibacterial factor in zinc oxide powder slurry. *Journal of fermentation bioengineering* 1998; 86:521-522.
15. Lu Y, Hao L, Hirakawa Y, Sato H: Antibacterial activity of TiO2/Ti composite photocatalyst films treated by ultrasonic cleaning. *Adv Mater Phys Chem* 2012; 2:9-12.
16. Petica A, Florea A, Gaidau C, Balan D, Anicai L: Synthesis and characterization of silver-titania nanocomposites prepared by electrochemical method with enhanced photocatalytic characteristics, antifungal and antimicrobial activity. *Journal of Materials Research Technology* 2019; 8:41-53.
17. He L, Liu Y, Mustapha A, Lin M: Antifungal activity of zinc oxide nanoparticles against Botrytis cinerea and Penicillium expansum. *Microbiol Res* 2011; 166:207-215.
18. Liu P, Luo L, Guo J, Liu H, Wang B, Deng B, Long CA, Cheng Y: Farnesol induces apoptosis and oxidative stress in the fungal pathogen Penicillium expansum. *Mycologia* 2010; 102:311-318.
19. Hammel KE, Kapich AN, Jensen Jr KA, Ryan ZC: Reactive oxygen species as agents of wood decay by fungi. *Enzyme microbial technology* 2002; 30:445-453.
20. Angle J, Dunn K, Wagner G: Effect of Cultural Practices on the Soil Population of Aspergillus flavus and Aspergillus parasiticus . *J Soil Science Society of America Journal* 1982; 46:301-304.
21. Bennett JW, Klich M: Mycotoxins. *Clin Microbiol Rev* 2003; 16:497-516.
22. Mozammel M, Ilkhechi NN, Ghezelbash B, Abad SNK: Antibacterial and heavy ion removal properties of La-and Ti-doped ZnO nanoparticles. *Materials Research Express* 2019; 6:085010.
23. Ilkhechi NN, Kaleji BK: High temperature stability and photocatalytic activity of nanocrystalline anatase powders with Zr and Si co-dopants. *Journal of sol-gel science technology* 2014; 69:351-356.
24. Kumar RS, Dananjaya S, De Zoysa M, Yang M: Enhanced antifungal activity of Ni-doped ZnO nanostructures under dark conditions. *RSC advances* 2016; 6:108468-108476.
25. Ilkhechi NN, Akbarpour MR, Yavari R, Azar Z: Sn 4+ and La 3+ co doped TiO 2 nanoparticles and their optical, photocatalytic and antibacterial properties under visible light. *Journal of Materials Science: Materials in Electronics* 2017; 28:16658-16664.
26. Agrawal M, Gupta S, Pich A, Zafeiropoulos NE, Stamm M: A facile approach to fabrication of ZnO–TiO2 hollow spheres. *J Chemistry of Materials* 2009; 21:5343-5348.

27. Li Y, Xie W, Hu X, Shen G, Zhou X, Xiang Y, Zhao X, Fang P: Comparison of dye photodegradation and its coupling with light-to-electricity conversion over TiO2 and ZnO. *Langmuir* 2010; 26:591-597.
28. Wang ZL, Kong XY, Zuo JM: Induced growth of asymmetric nanocantilever arrays on polar surfaces. *Phys Rev Lett* 2003; 91:185502.
29. Ilkhechi NN, Kaleji BK: Optical and structure properties of nanocrystalline titania powders with Cu dopant. *Silicon* 2017; 9:285-291.
30. Ilkhechi NN, Koozegar-Kaleji B, Dousi F: Optical and structural properties of tenorite nanopowders doped by Si and Zr. *Optical Quantum Electronics* 2015; 47:633-642.
31. Gholami M, Shirzad-Siboni M, Farzadkia M, Yang J-K: Synthesis, characterization, and application of ZnO/TiO2 nanocomposite for photocatalysis of a herbicide (Bentazon). *J Desalination water treatment* 2016; 57:13632-13644.
32. Chakra CS, Rajendar V, Rao KV, Kumar M: Enhanced antimicrobial and anticancer properties of ZnO and TiO 2 nanocomposites. *3 Biotech* 2017; 7:89.
33. Adams LK, Lyon DY, Alvarez PJ: Comparative eco-toxicity of nanoscale TiO2, SiO2, and ZnO water suspensions. *Water Res* 2006; 40:3527-3532.
34. Maneerat C, Hayata Y: Antifungal activity of TiO2 photocatalysis against Penicillium expansum in vitro and in fruit tests. *Int J Food Microbiol* 2006; 107:99-103.
35. Fathima AF, Mani RJ, Sakthipandi K, Manimala K, Hossain A, Materials: Enhanced Antifungal Activity of Pure and Iron-Doped ZnO Nanoparticles Prepared in the Absence of Reducing Agents. *Journal of Inorganic Organometallic Polymers* 2019:1-9.
36. Sharon A, Finkelstein A, Shlezinger N, Hatam I: Fungal apoptosis: function, genes and gene function. *FEMS Microbiol Rev* 2009; 33:833-854.
37. Kumar KM, Mandal BK, Naidu EA, Sinha M, Kumar KS, Reddy PS: Synthesis and characterisation of flower shaped zinc oxide nanostructures and its antimicrobial activity. *Spectrochimica Acta Part A: Molecular Biomolecular Spectroscopy* 2013; 104:171-174.
38. Mitoraj D, Janczyk A, Strus M, Kisch H, Stochel G, Heczko PB, Macyk W: Visible light inactivation of bacteria and fungi by modified titanium dioxide. *Photochem Photobiol Sci* 2007; 6:642-648.

Figures

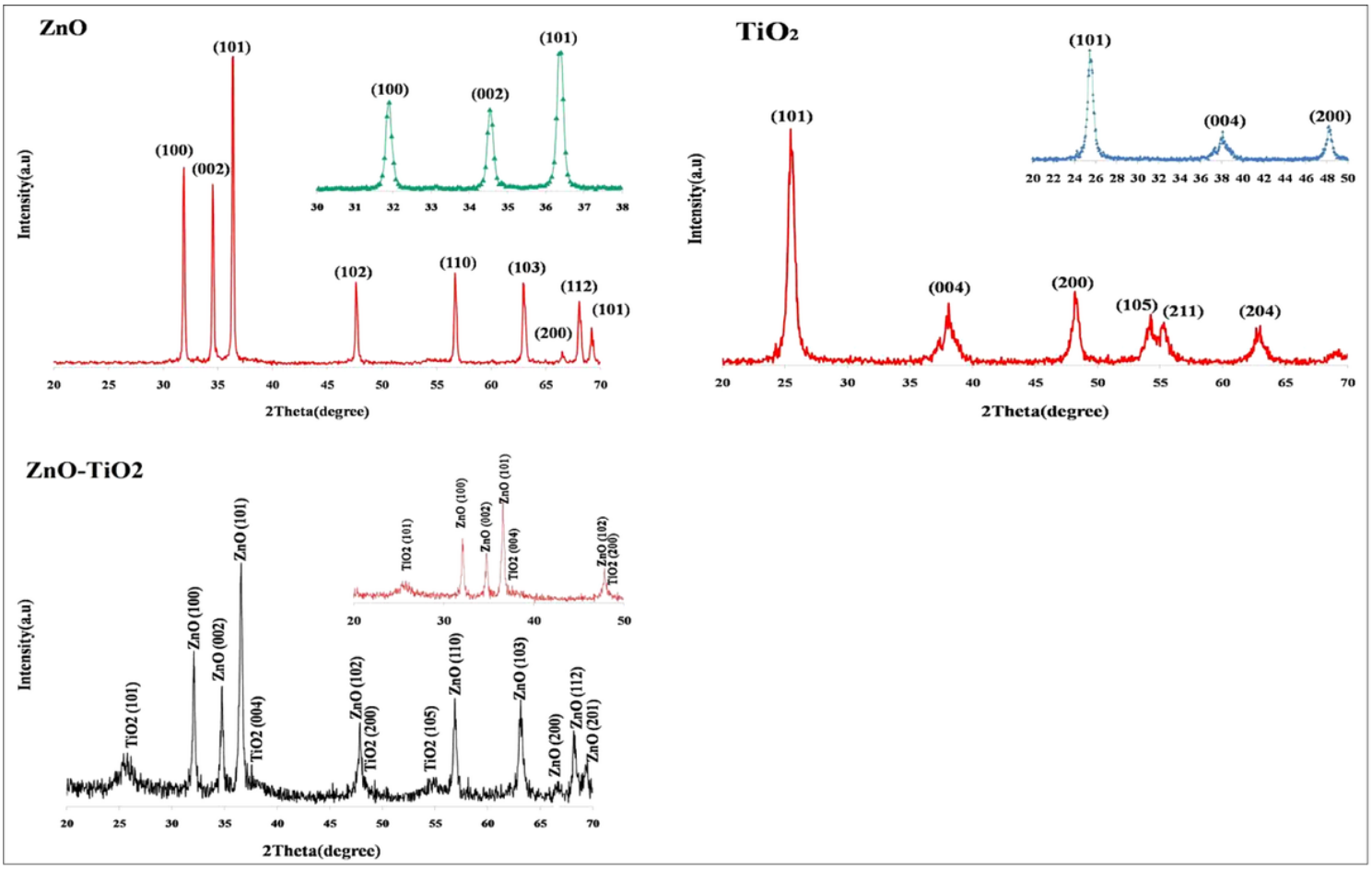

Figure 1

The XRD pattern of ZnO, TiO2, and ZnO-TiO2 nanopowders

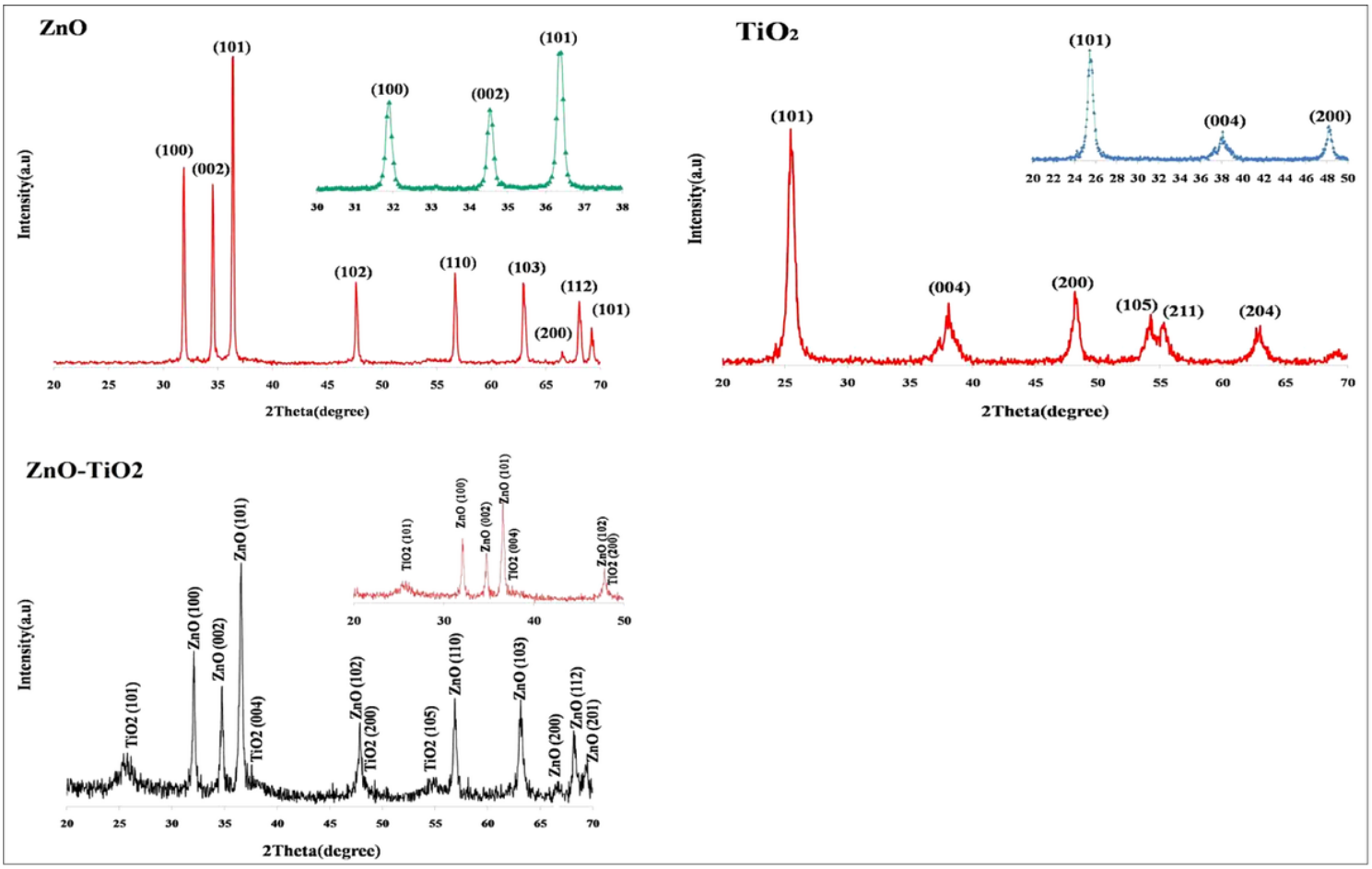

Figure 1

The XRD pattern of ZnO, TiO2, and ZnO-TiO2 nanopowders

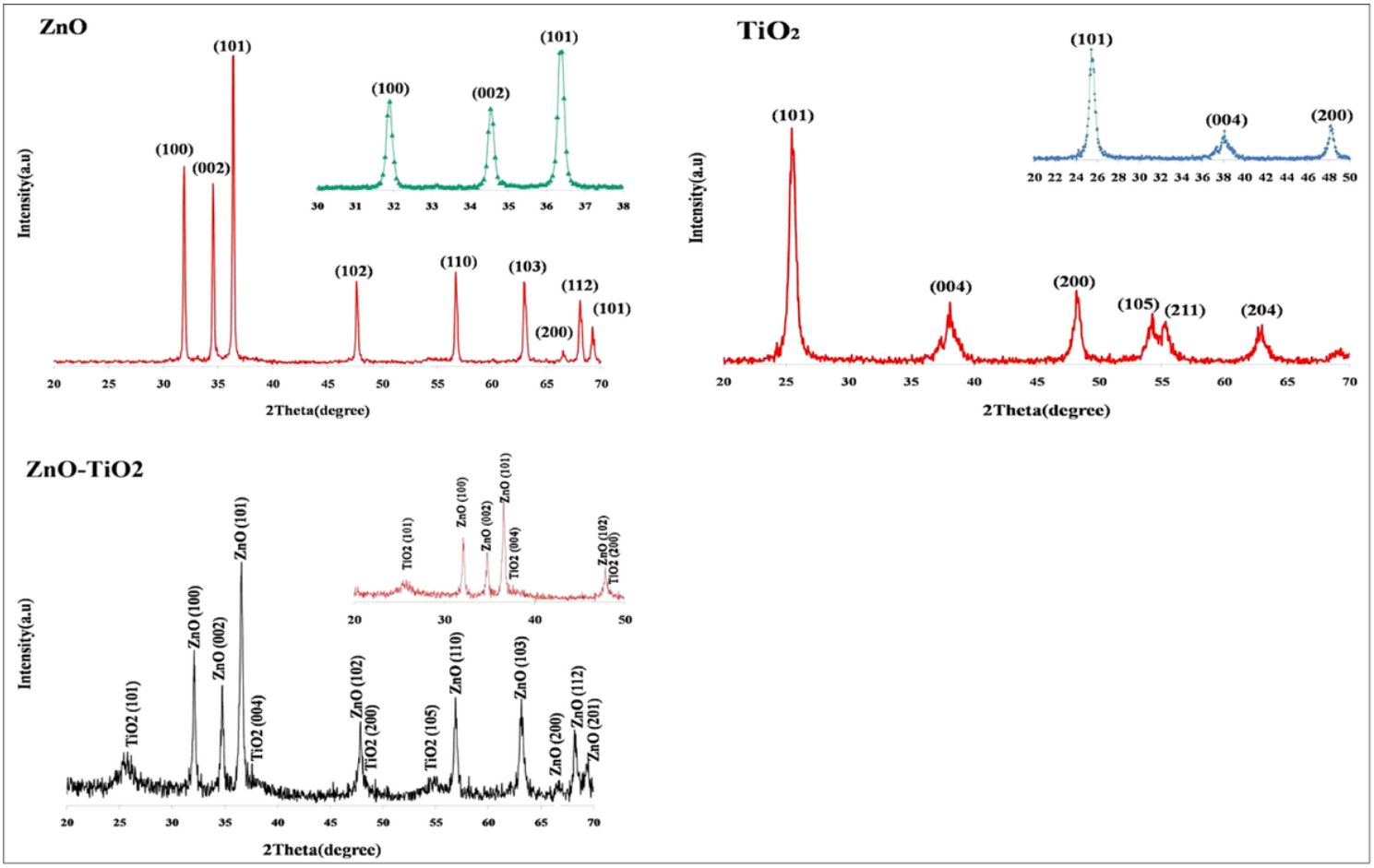

Figure 1

The XRD pattern of ZnO, TiO2, and ZnO-TiO2 nanopowders

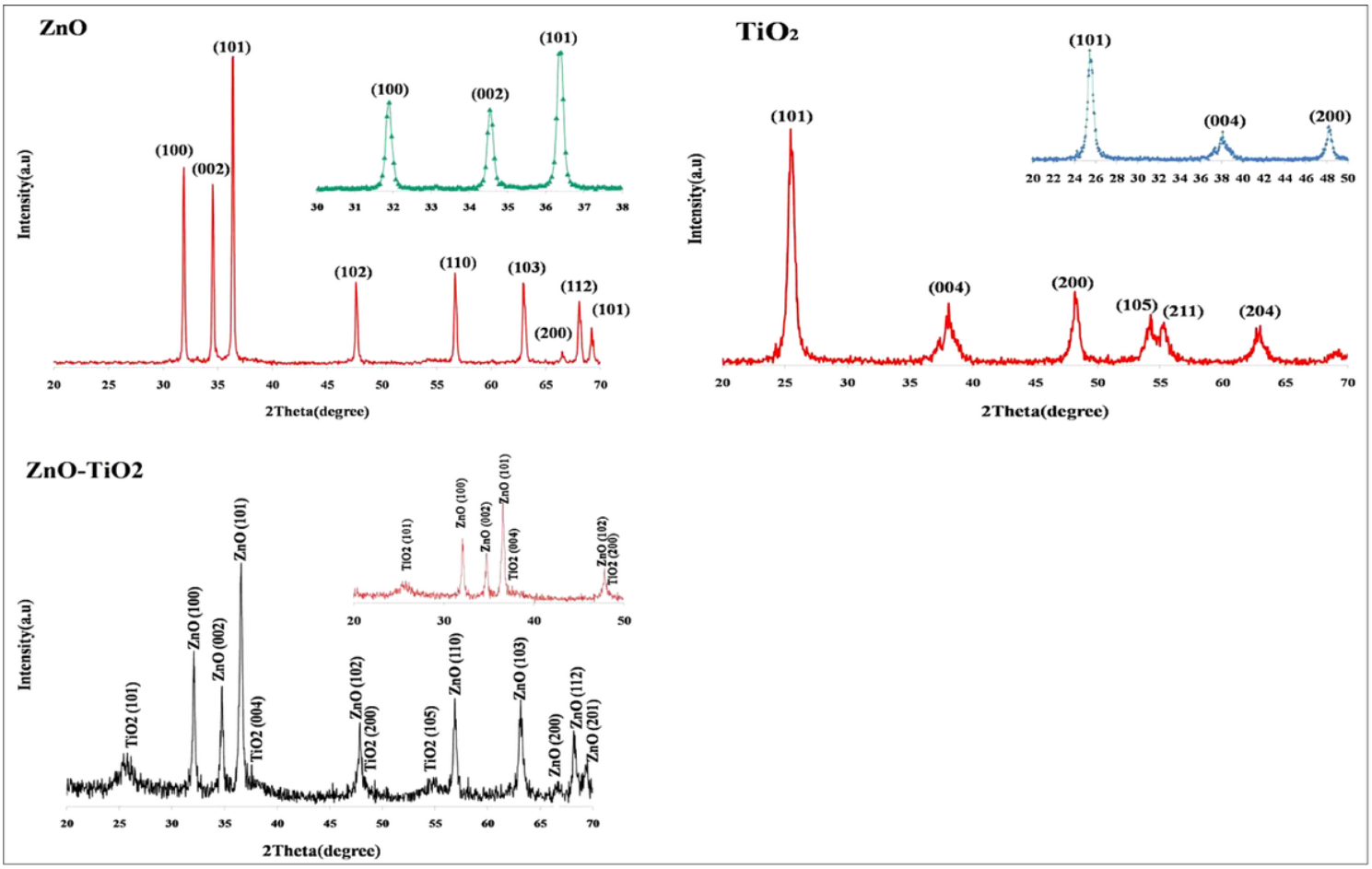

Figure 1

The XRD pattern of ZnO, TiO2, and ZnO-TiO2 nanopowders

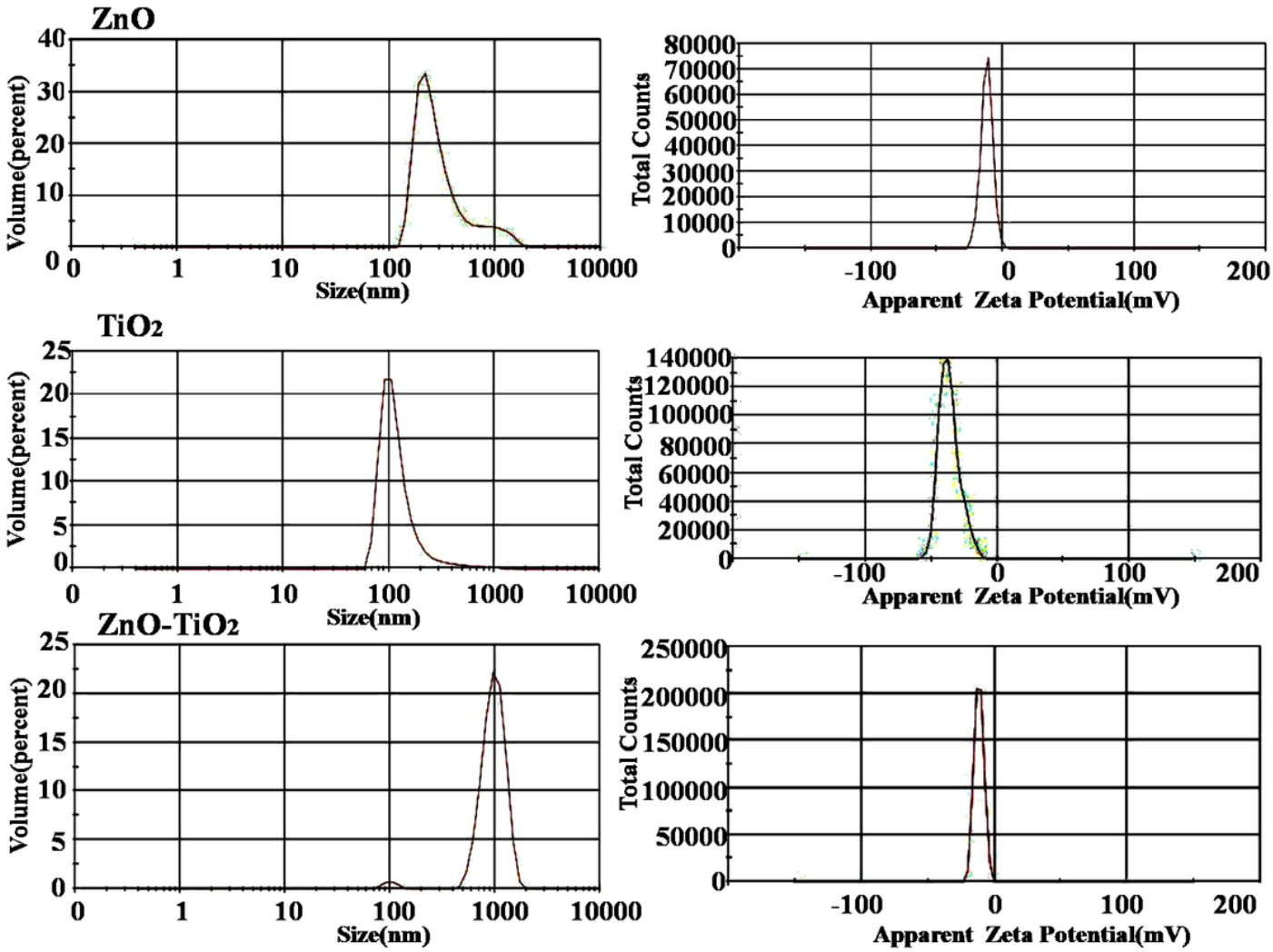

Figure 2

PSA and zeta potential of ZnO, TiO2, and ZnO-TiO2 nanoparticles

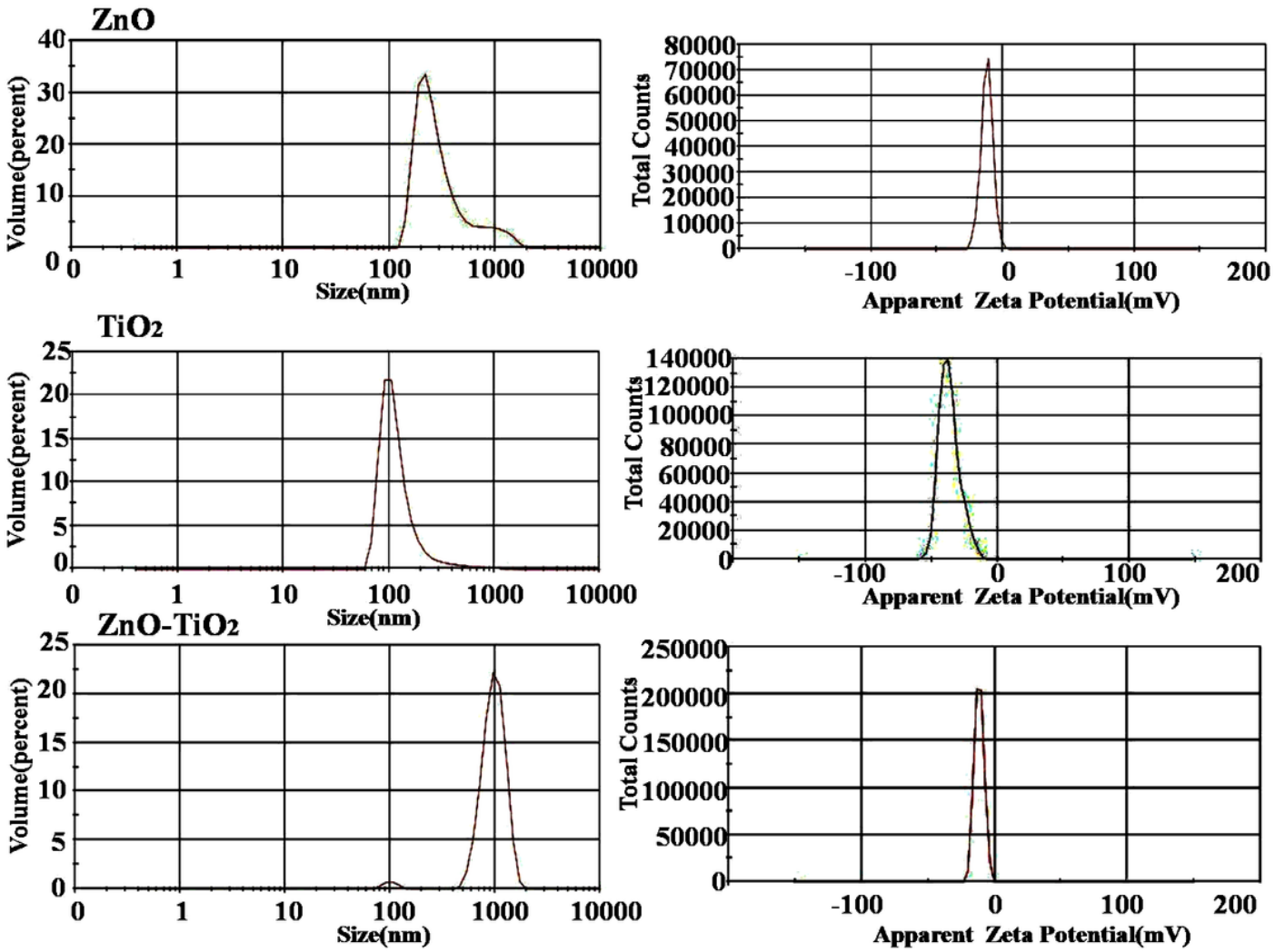

Figure 2

PSA and zeta potential of ZnO, TiO2, and ZnO-TiO2 nanoparticles

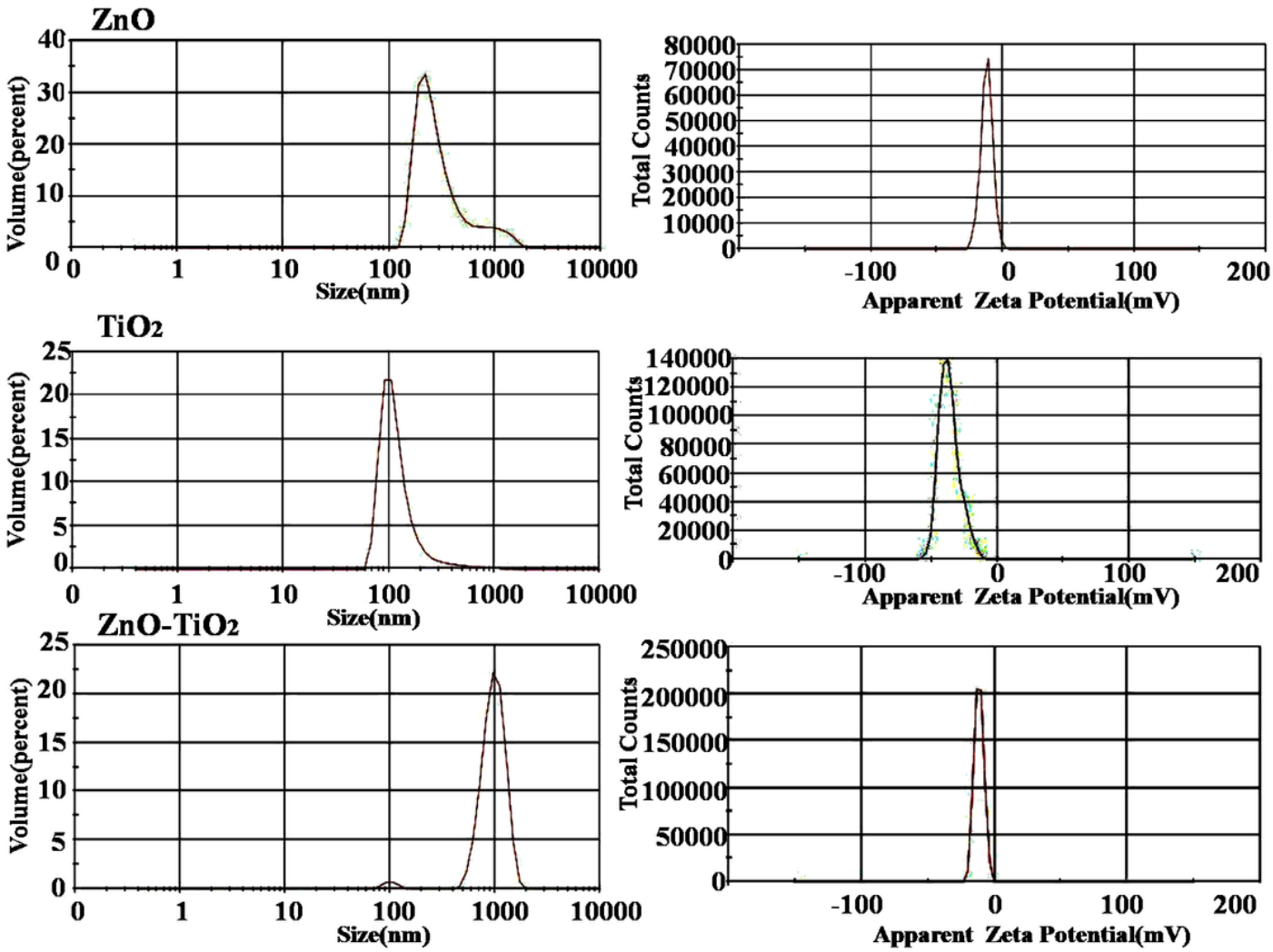

Figure 2

PSA and zeta potential of ZnO, TiO2, and ZnO-TiO2 nanoparticles

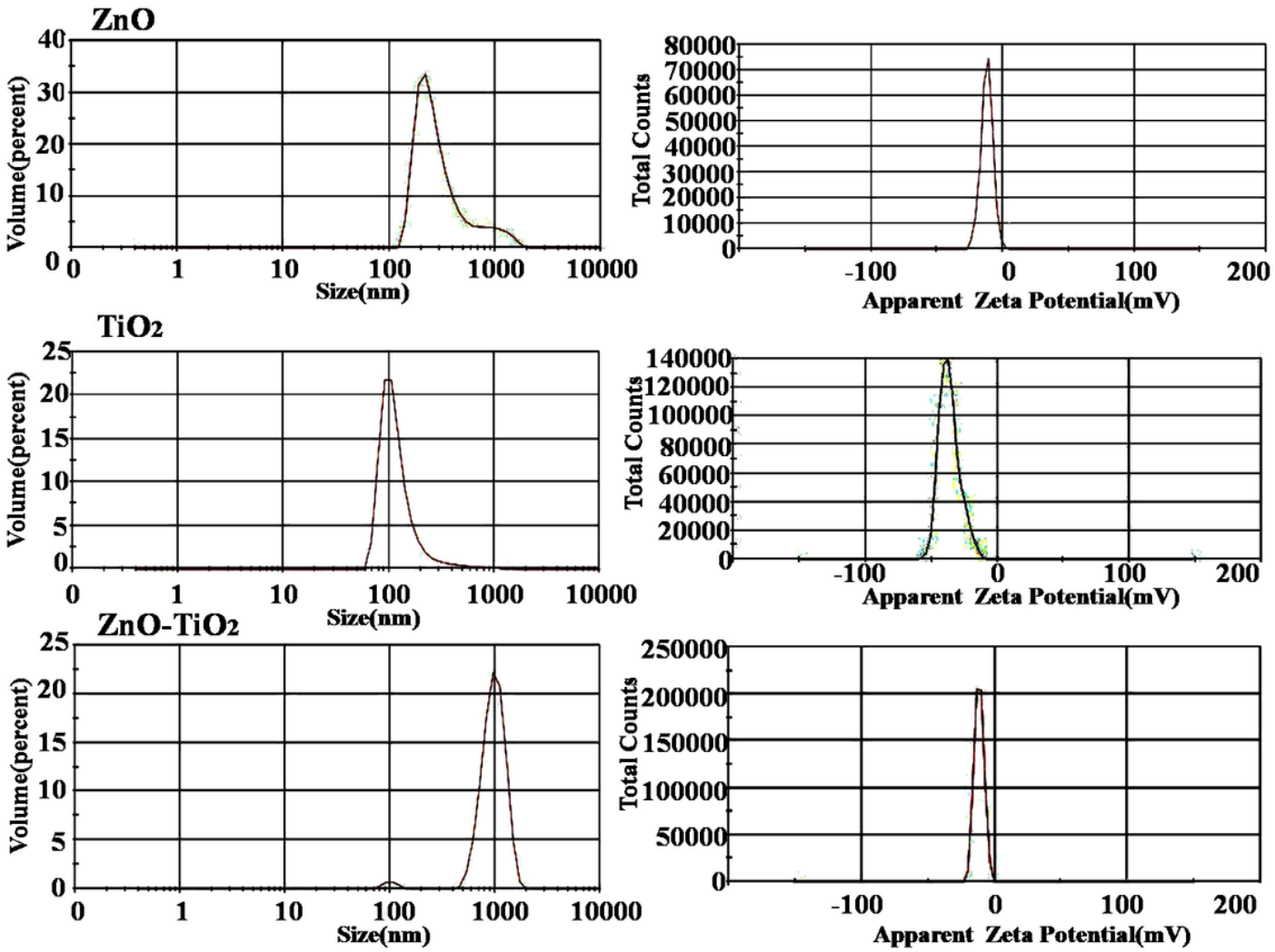

Figure 2

PSA and zeta potential of ZnO, TiO2, and ZnO-TiO2 nanoparticles

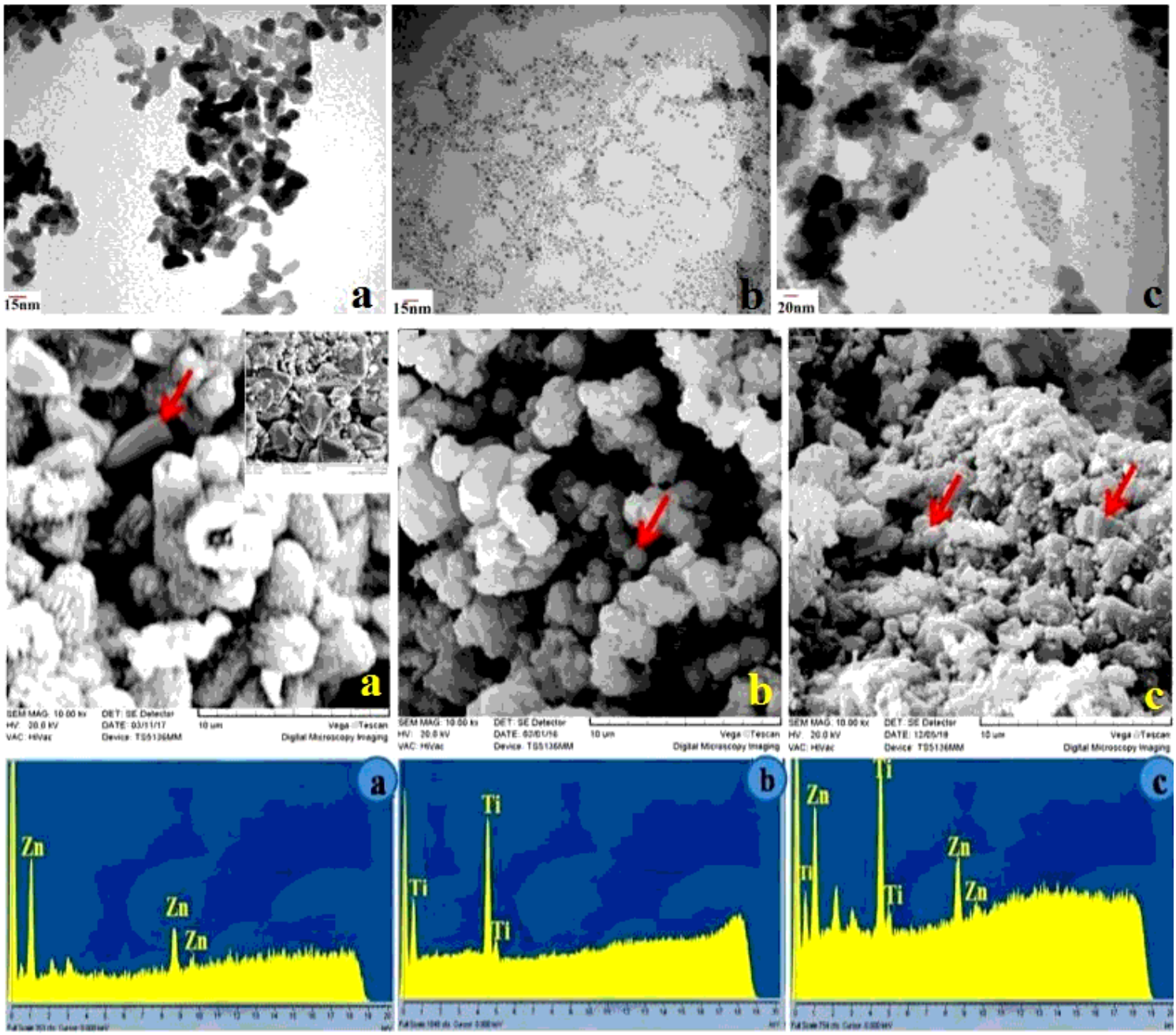

Figure 3

TEM, SEM, and EDX images of nanostructures images of nanopowders. a) ZnO; b) TiO2; c) ZnO-TiO2

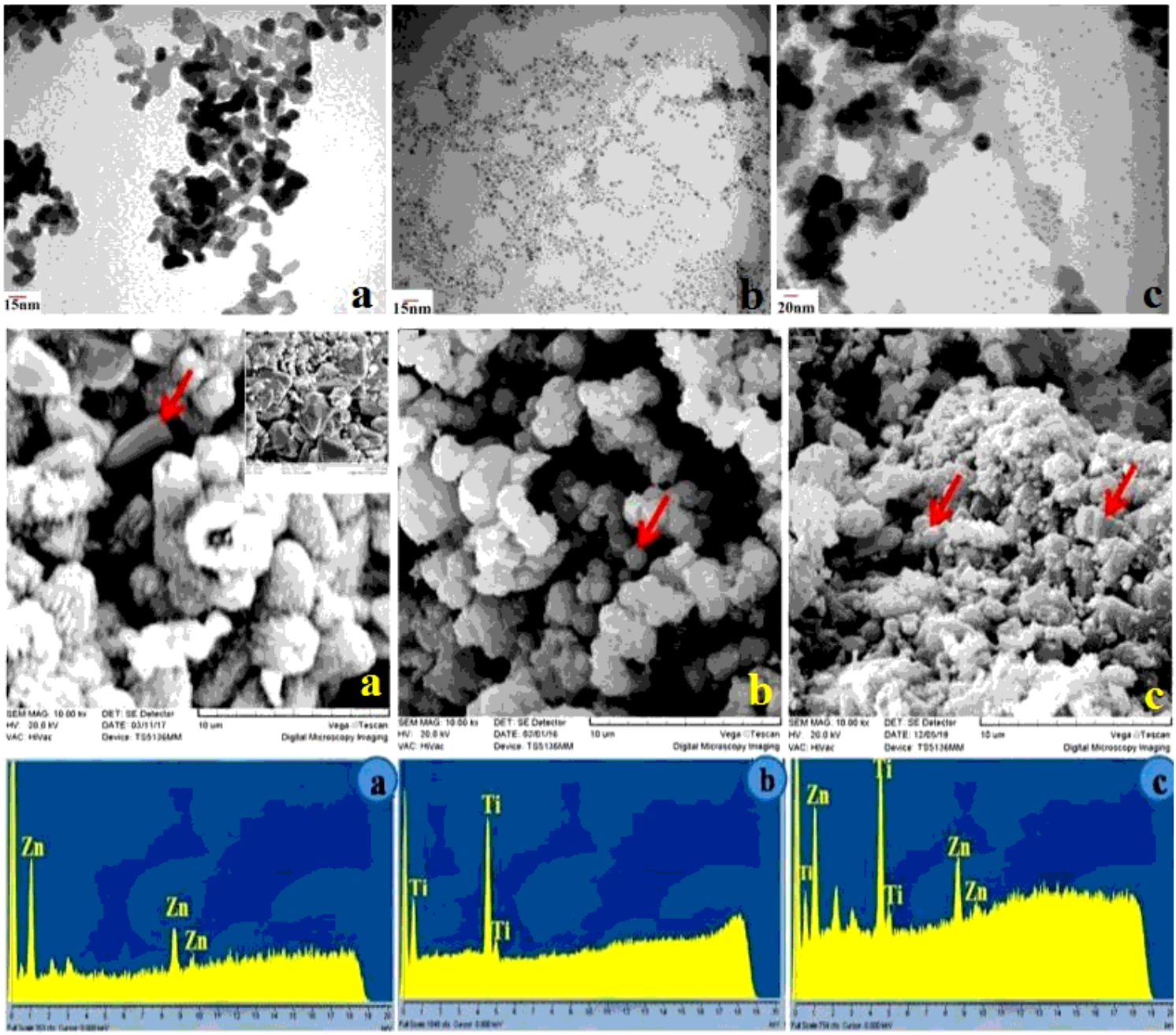

Figure 3

TEM, SEM, and EDX images of nanostructures images of nanopowders. a) ZnO; b) TiO2; c) ZnO-TiO2

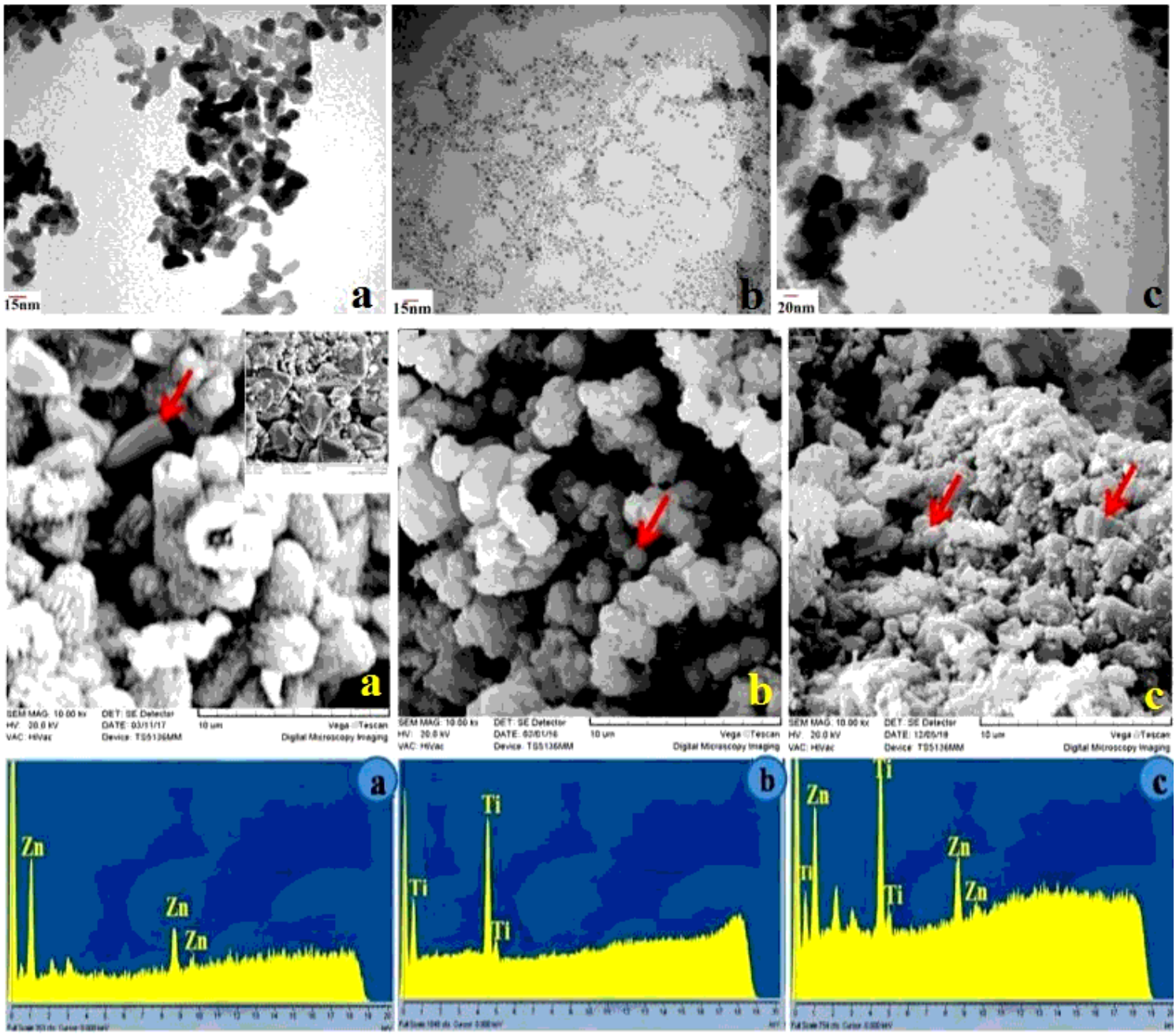

Figure 3

TEM, SEM, and EDX images of nanostructures images of nanopowders. a) ZnO; b) TiO2; c) ZnO-TiO2

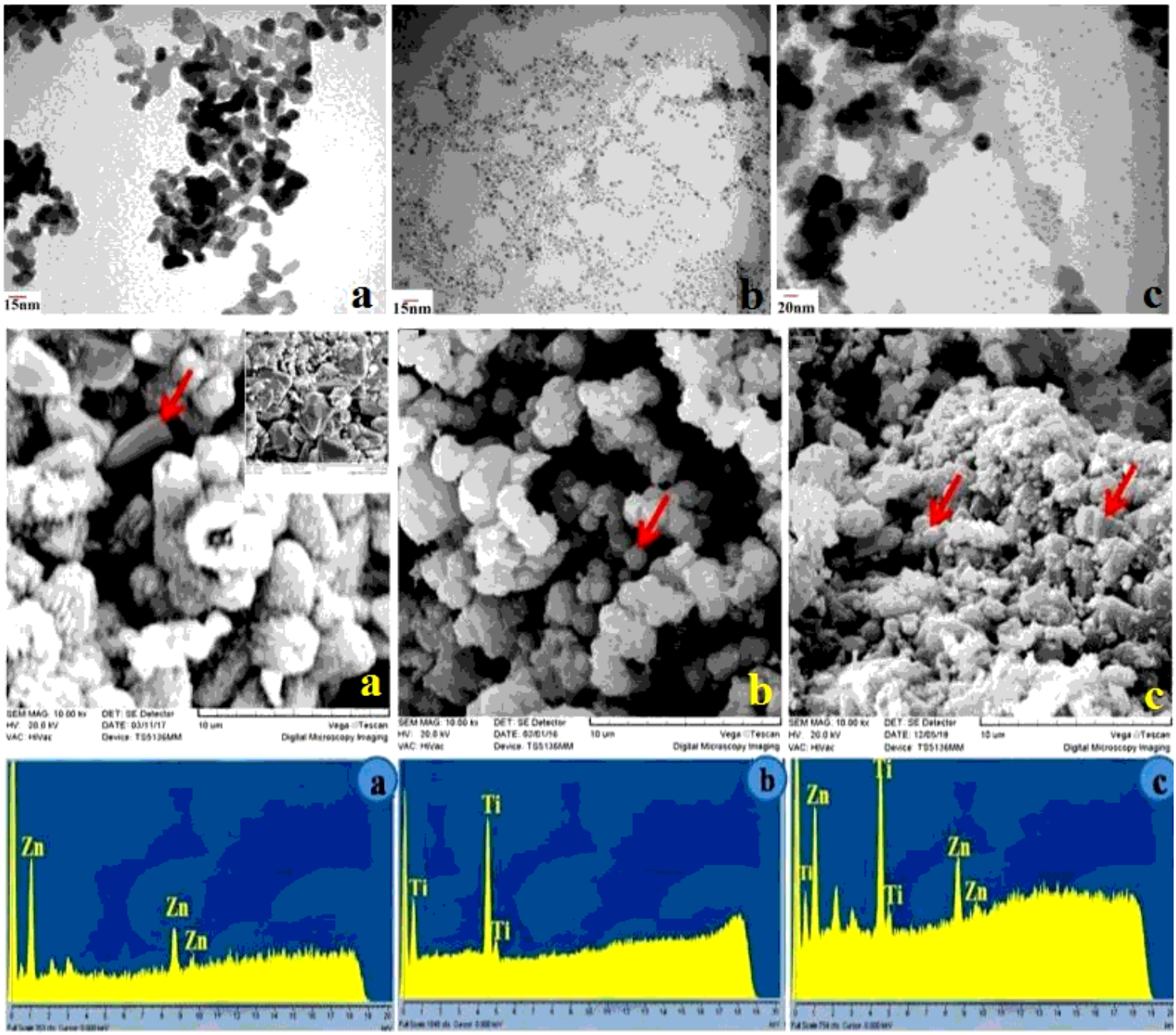

Figure 3

TEM, SEM, and EDX images of nanostructures images of nanopowders. a) ZnO; b) TiO2; c) ZnO-TiO2

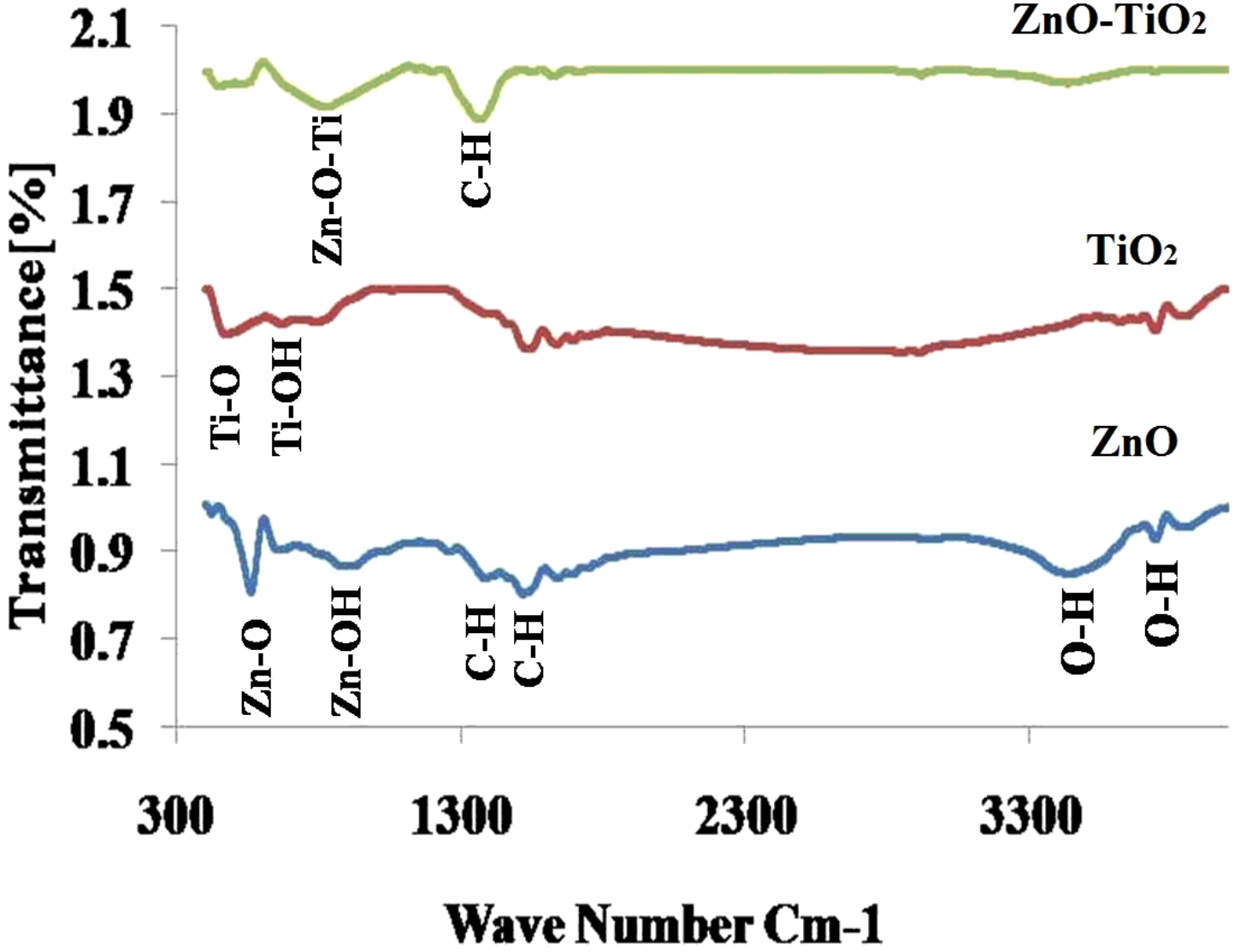

Figure 4

The FTIR analysis of nanoparticles

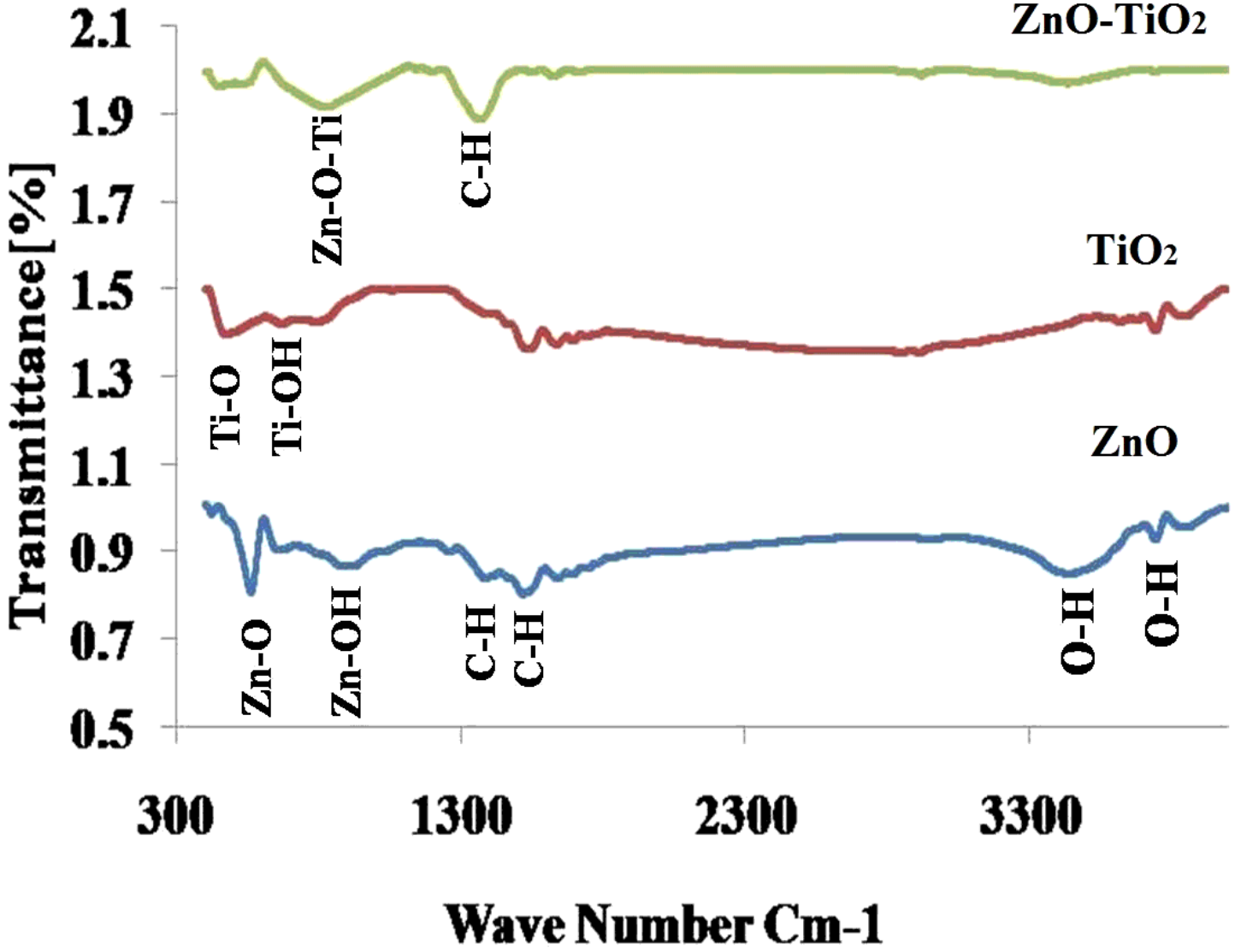

Figure 4

The FTIR analysis of nanoparticles

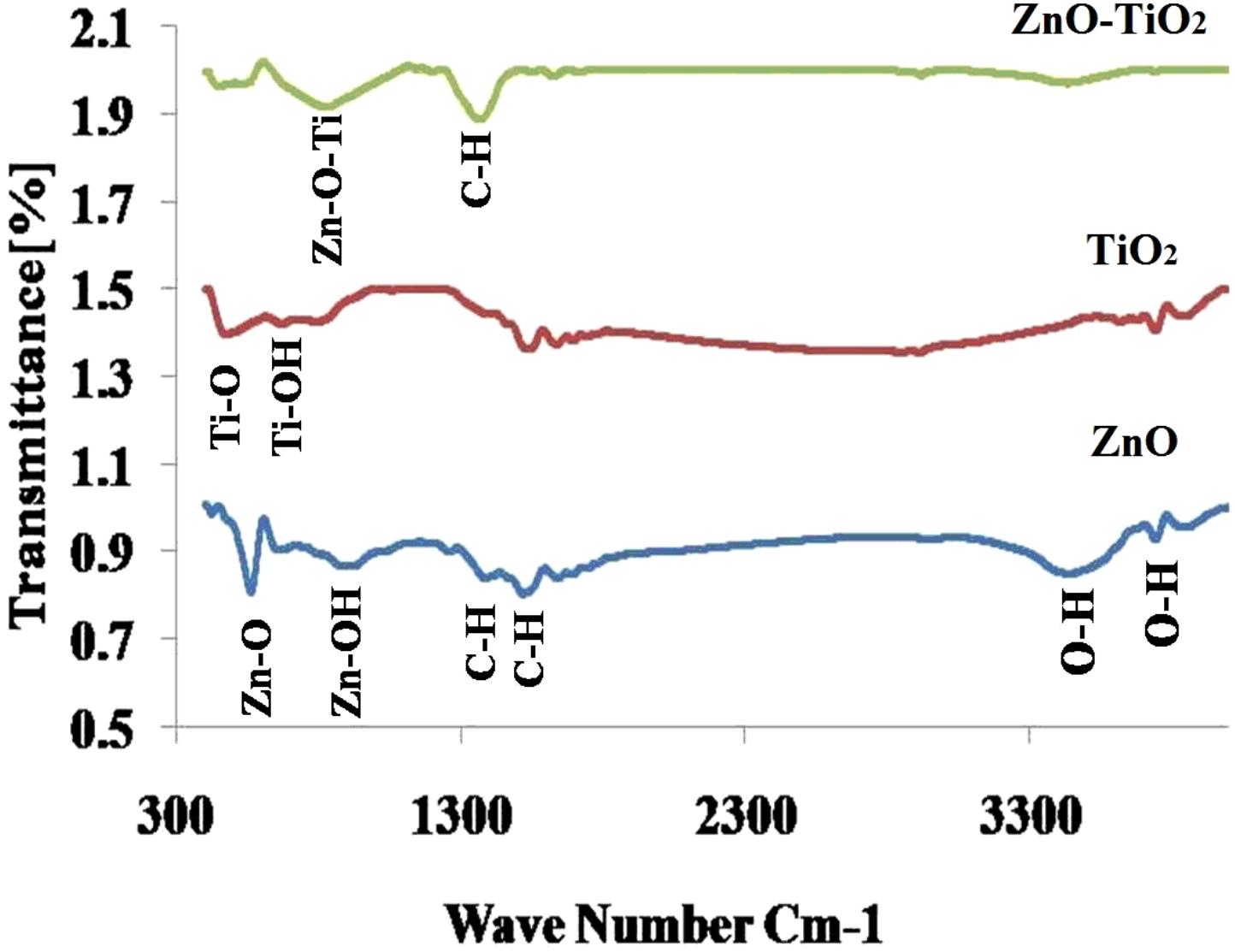

Figure 4

The FTIR analysis of nanoparticles

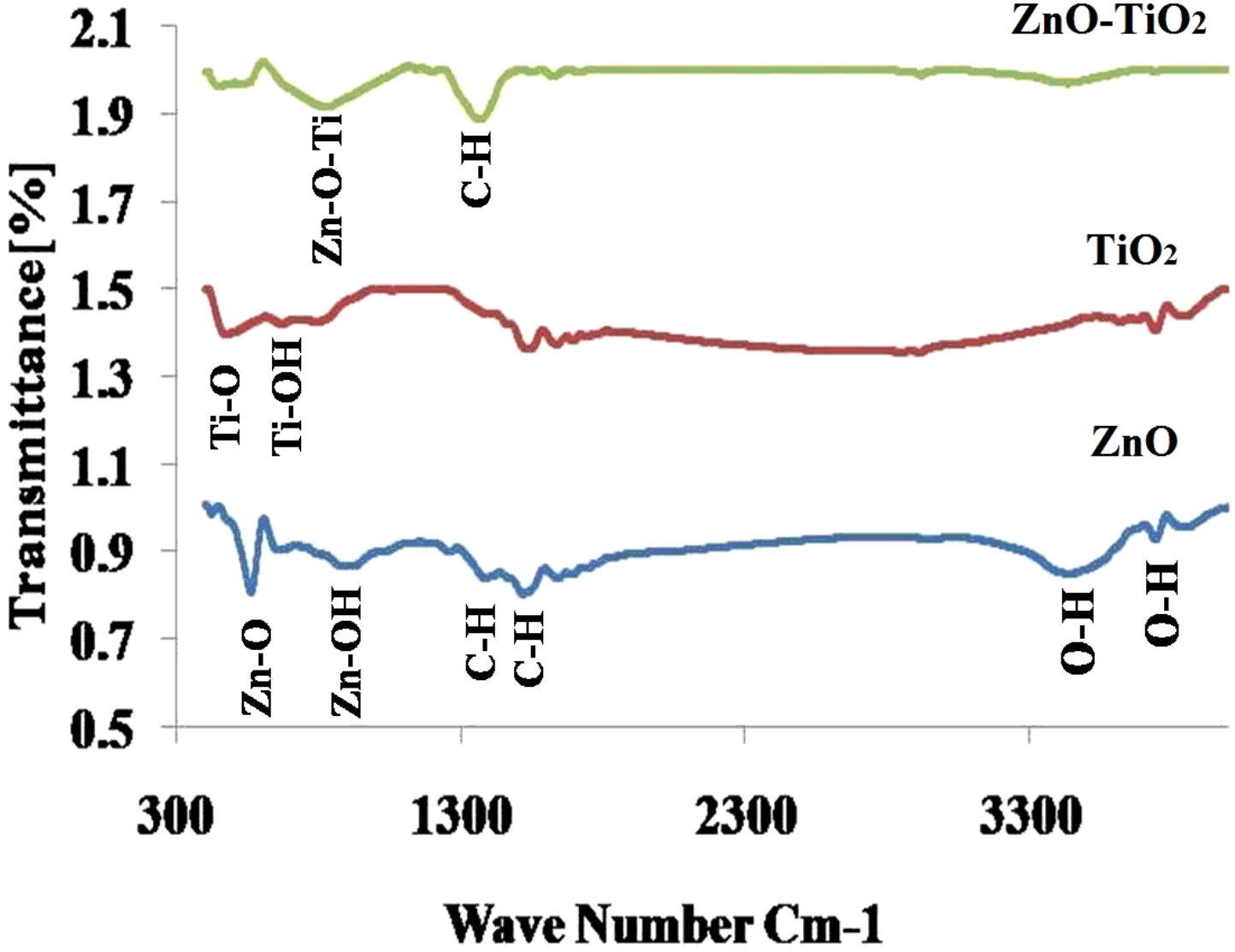

Figure 4

The FTIR analysis of nanoparticles

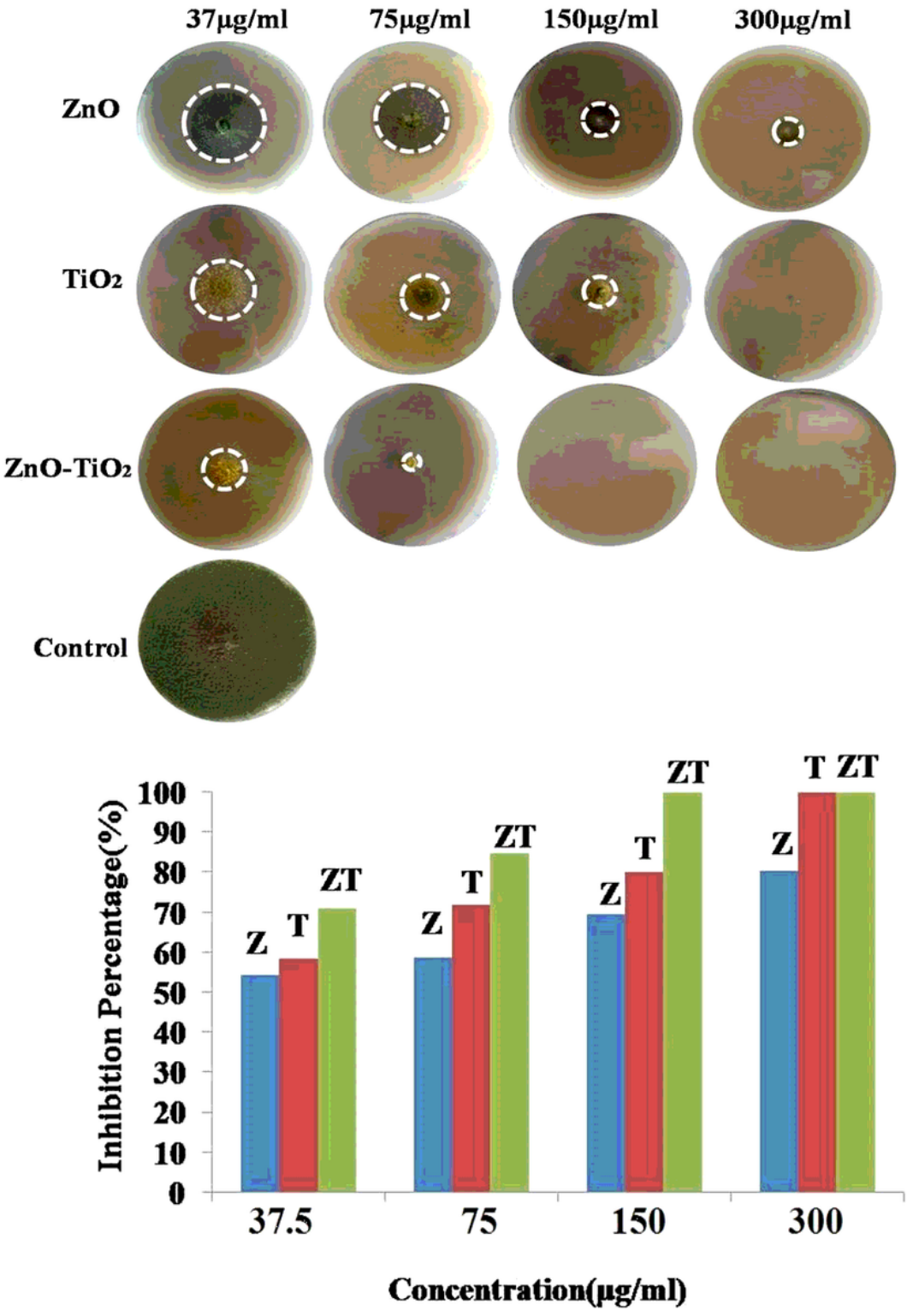

Figure 5

The Fungicidal inhibition zone for ZnO, TiO2, and ZnO-TiO2 nanoparticles against A. flavus

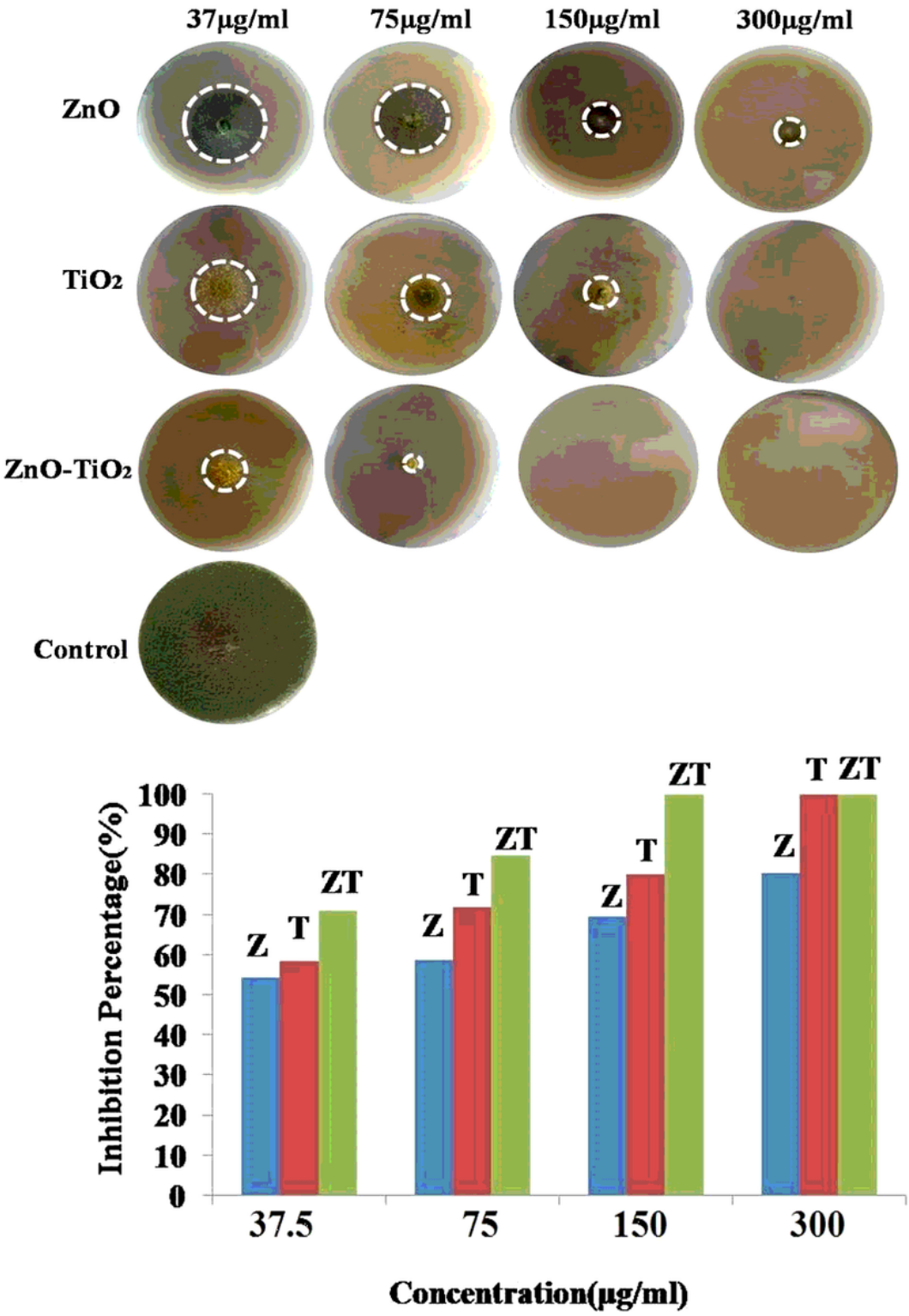

Figure 5

The Fungicidal inhibition zone for ZnO, TiO2, and ZnO-TiO2 nanoparticles against A. flavus

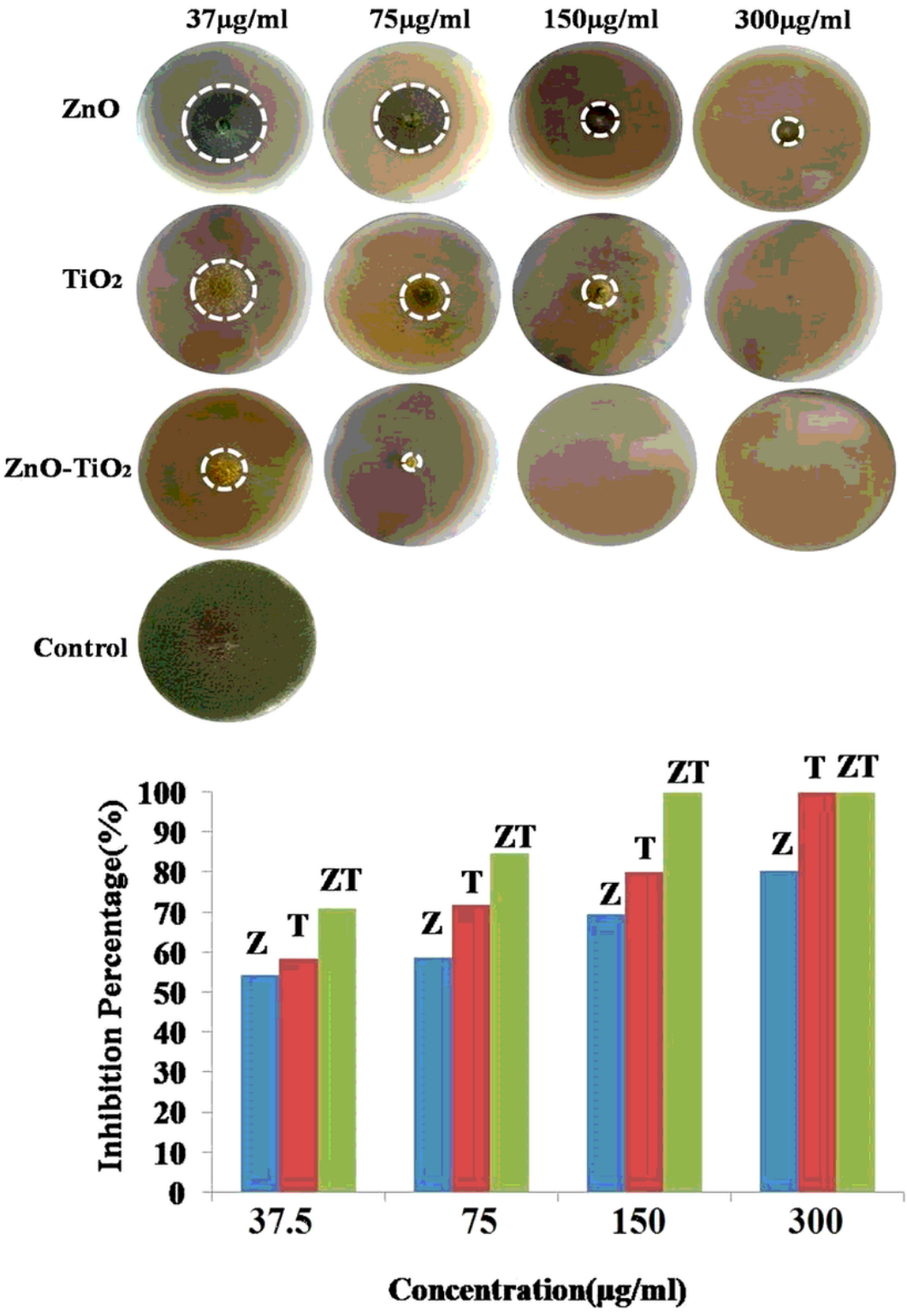

Figure 5

The Fungicidal inhibition zone for ZnO, TiO2, and ZnO-TiO2 nanoparticles against A. flavus

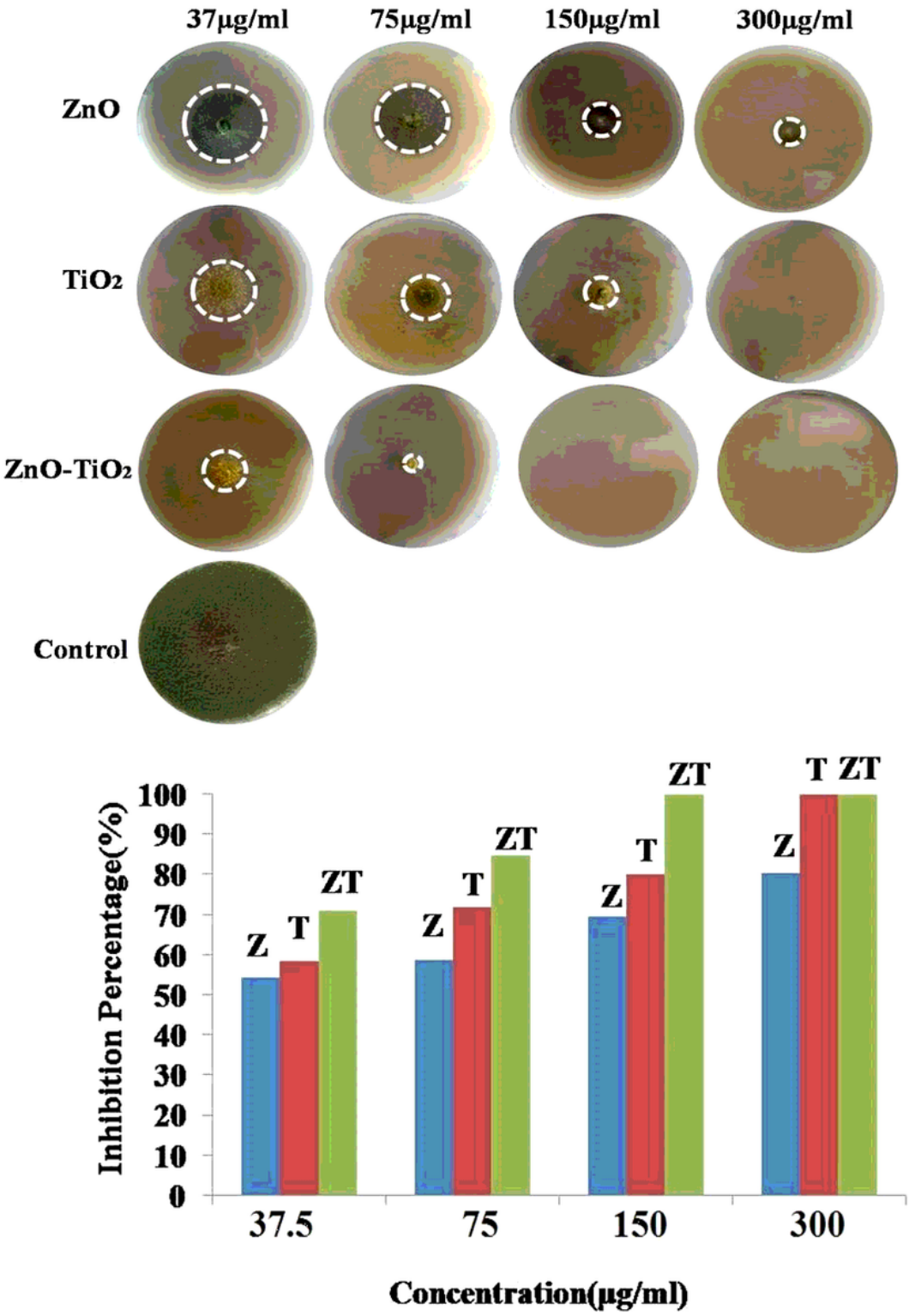

Figure 5

The Fungicidal inhibition zone for ZnO, TiO2, and ZnO-TiO2 nanoparticles against A. flavus

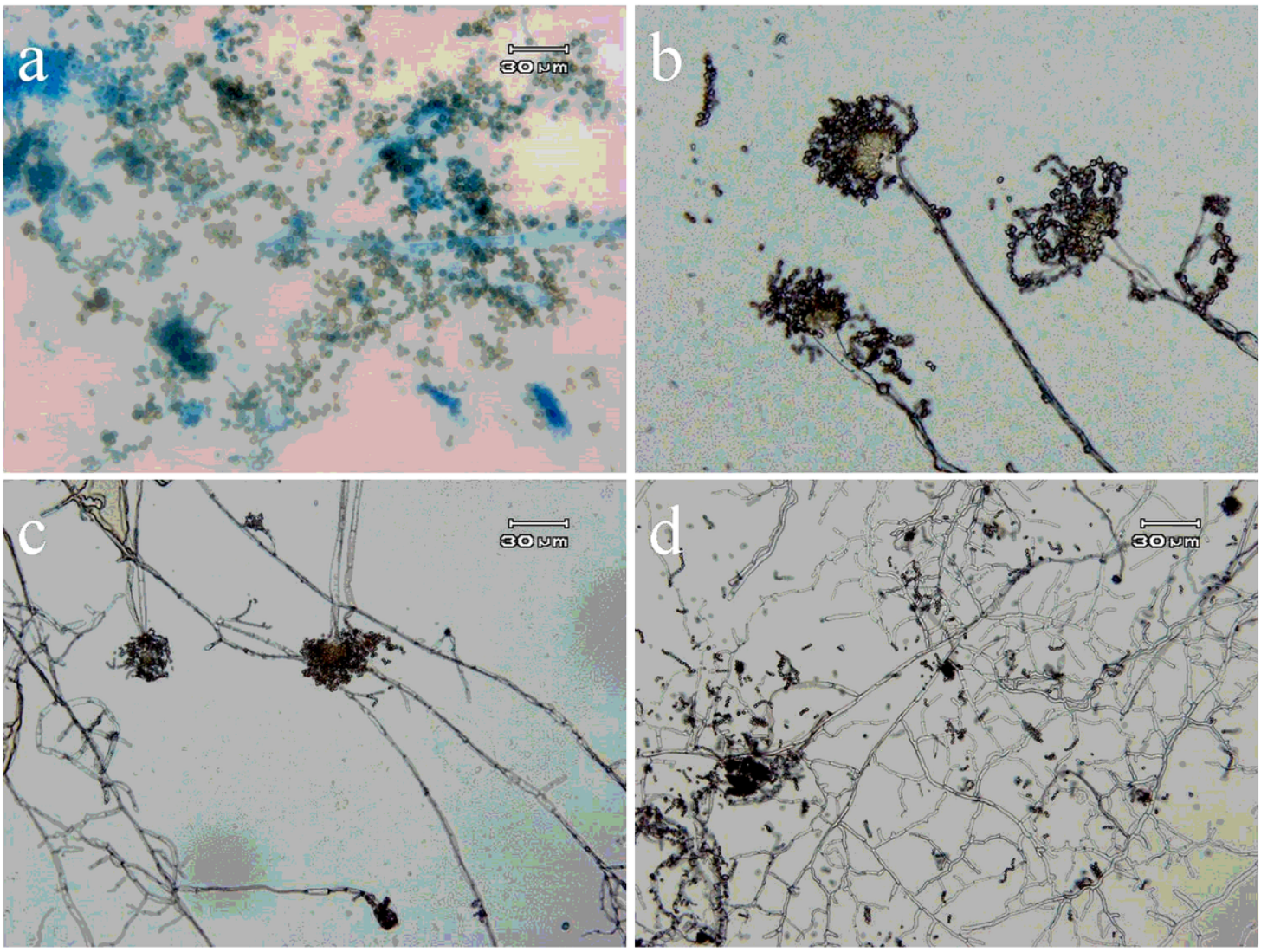

Figure 6

Light microscopy images of treated and untreated A. flavus . a) Control, b) Treated by ZnO, c) Treated by TiO2, and d) Treated by ZnO-TiO2

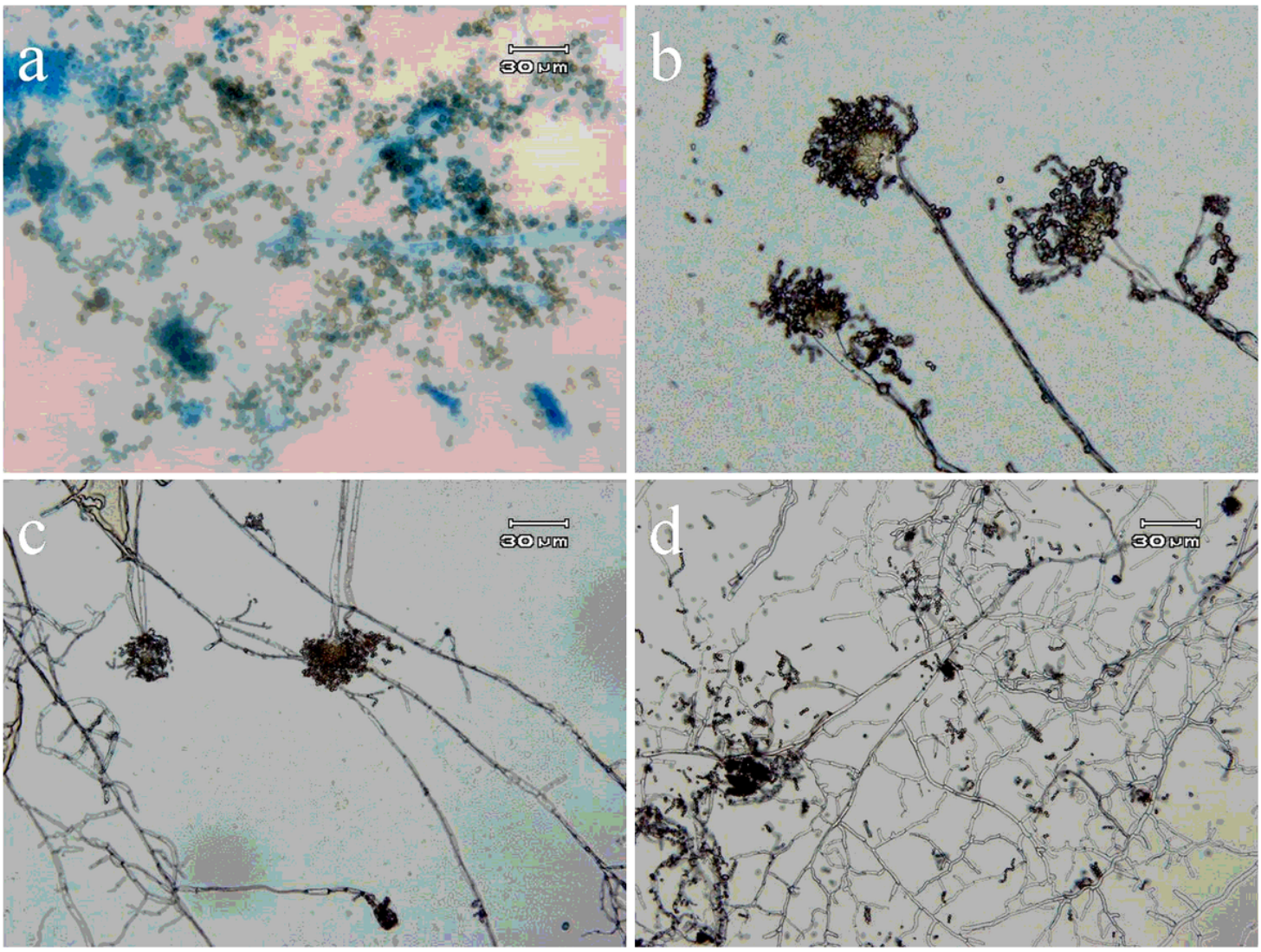

Figure 6

Light microscopy images of treated and untreated A. flavus . a) Control, b) Treated by ZnO, c) Treated by TiO2, and d) Treated by ZnO-TiO2

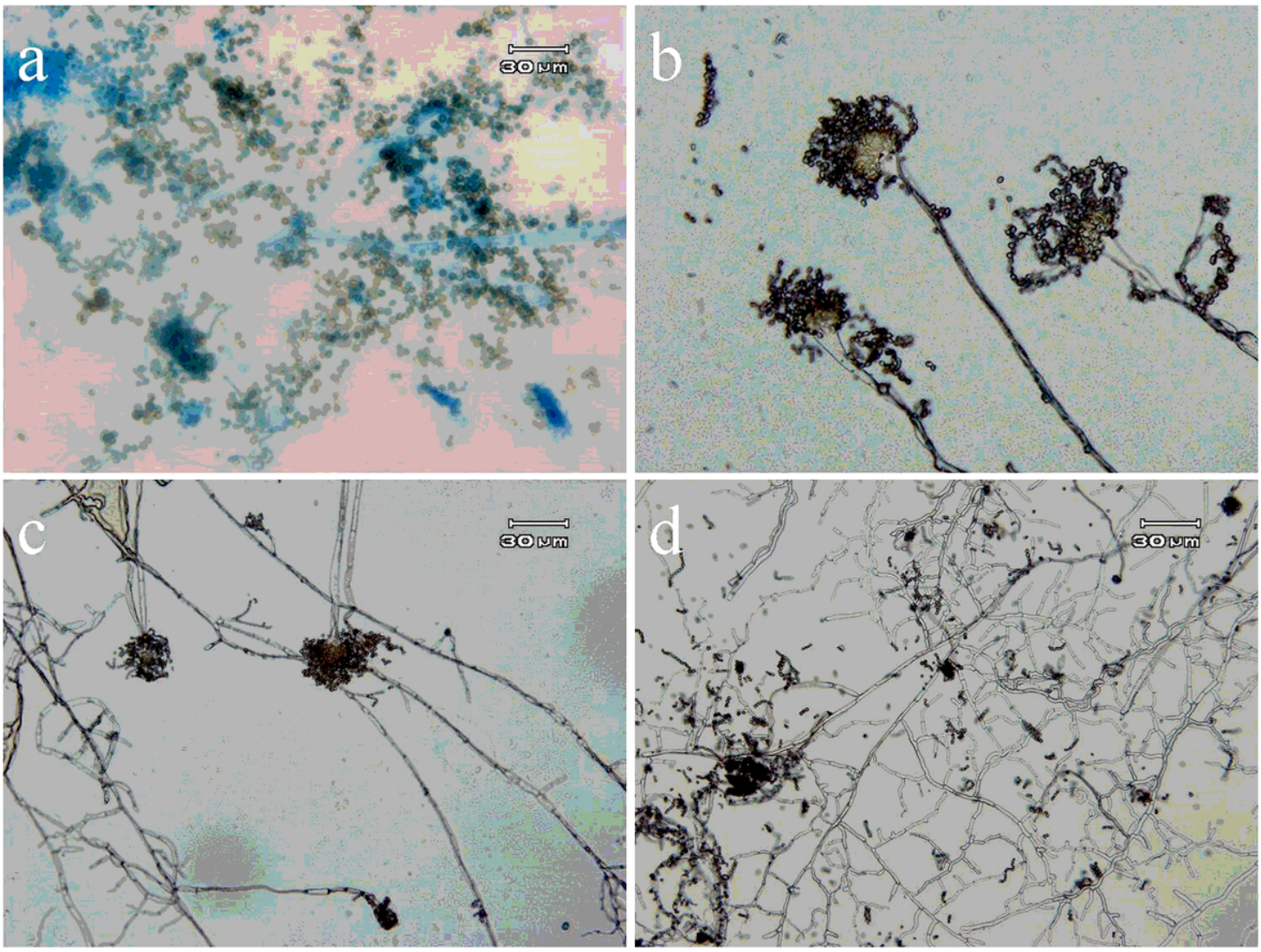

Figure 6

Light microscopy images of treated and untreated A. flavus . a) Control, b) Treated by ZnO, c) Treated by TiO2, and d) Treated by ZnO-TiO2

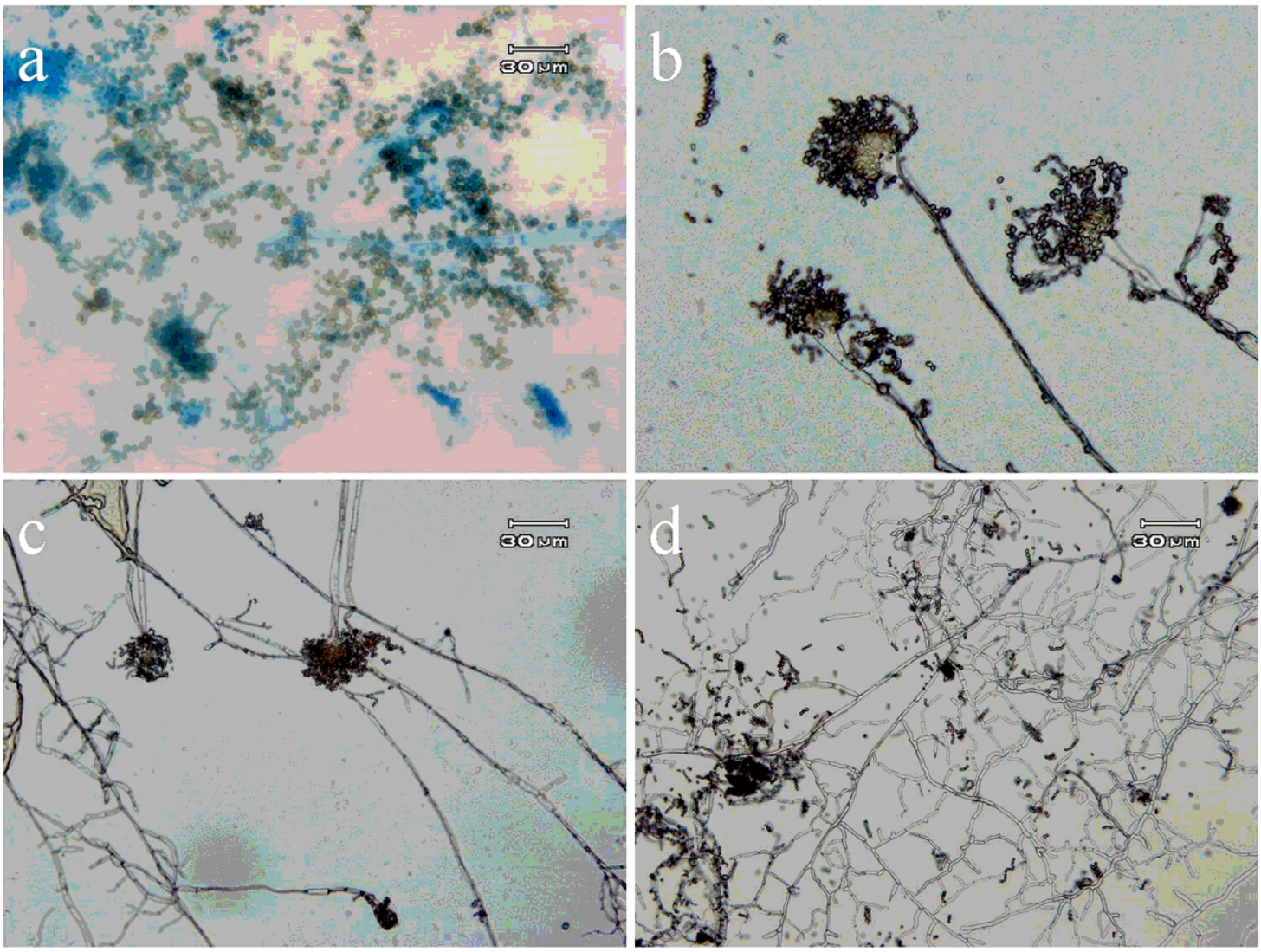

Figure 6

Light microscopy images of treated and untreated A. flavus . a) Control, b) Treated by ZnO, c) Treated by TiO2, and d) Treated by ZnO-TiO2

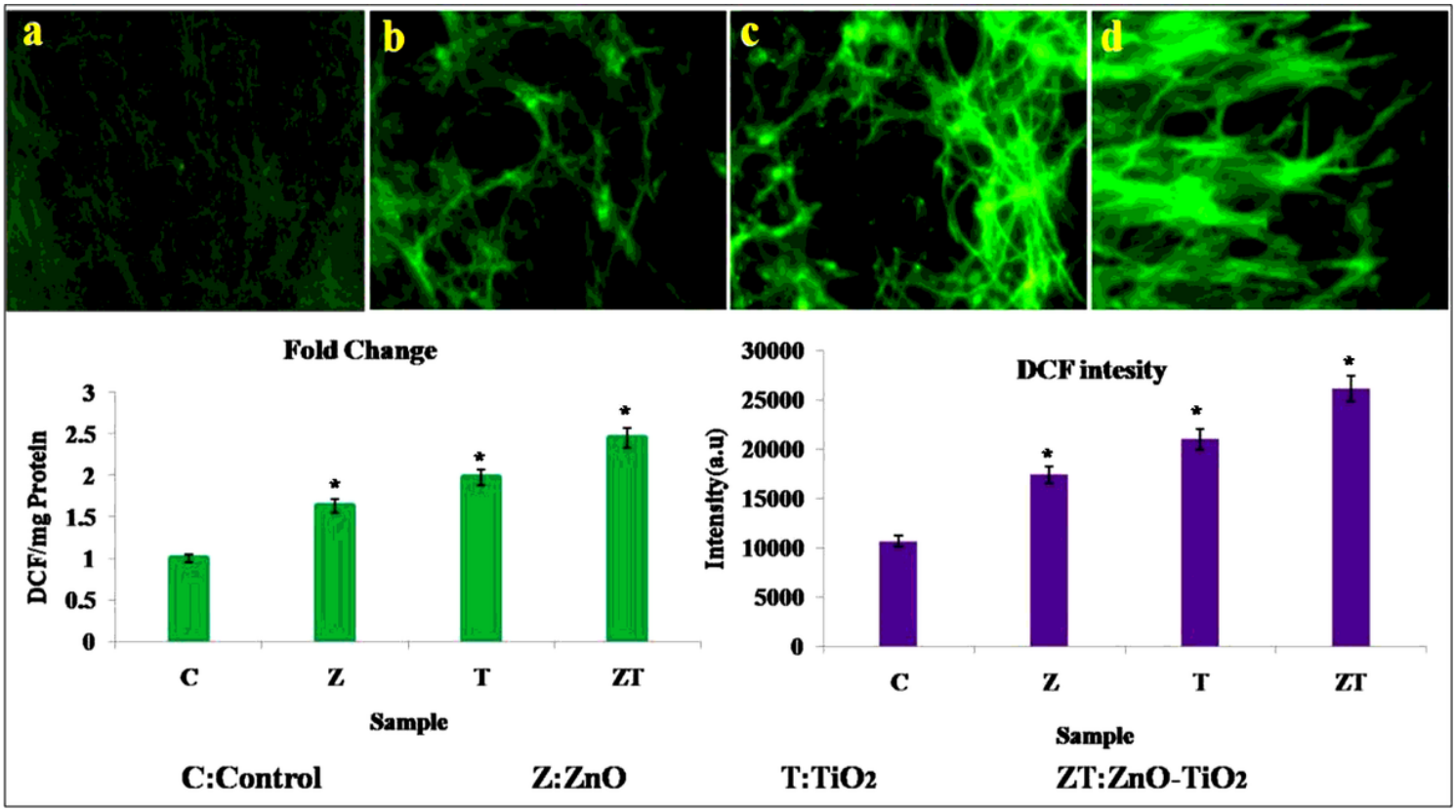

Figure 7

ROS detection of nanostructures by DCFH-DA methodology. Panels a) untreated control, b) ZnO, c) TiO2, and d) ZnO-TiO2 treated A. flavus

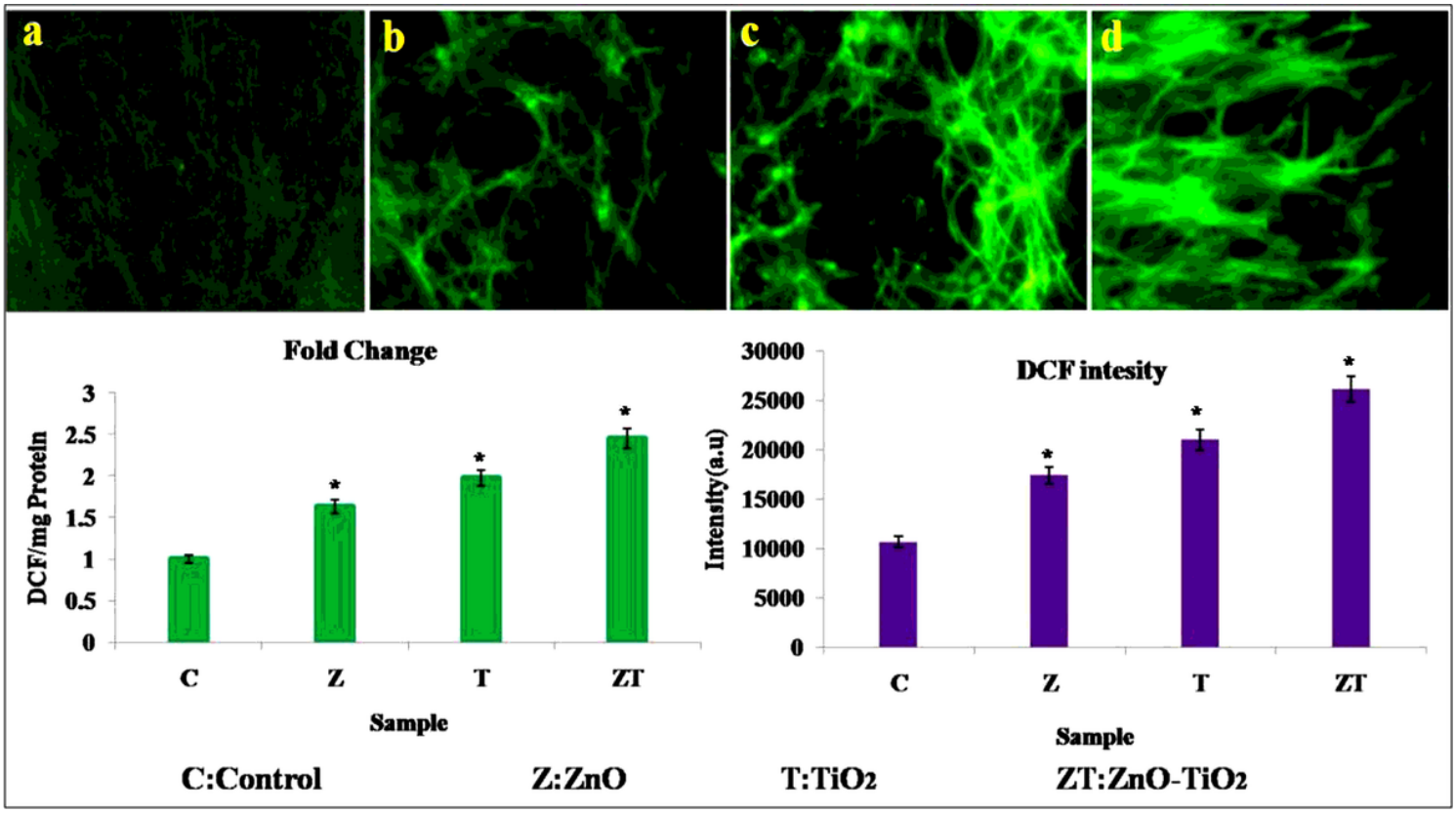

Figure 7

ROS detection of nanostructures by DCFH-DA methodology. Panels a) untreated control, b) ZnO, c) TiO2, and d) ZnO-TiO2 treated A. flavus

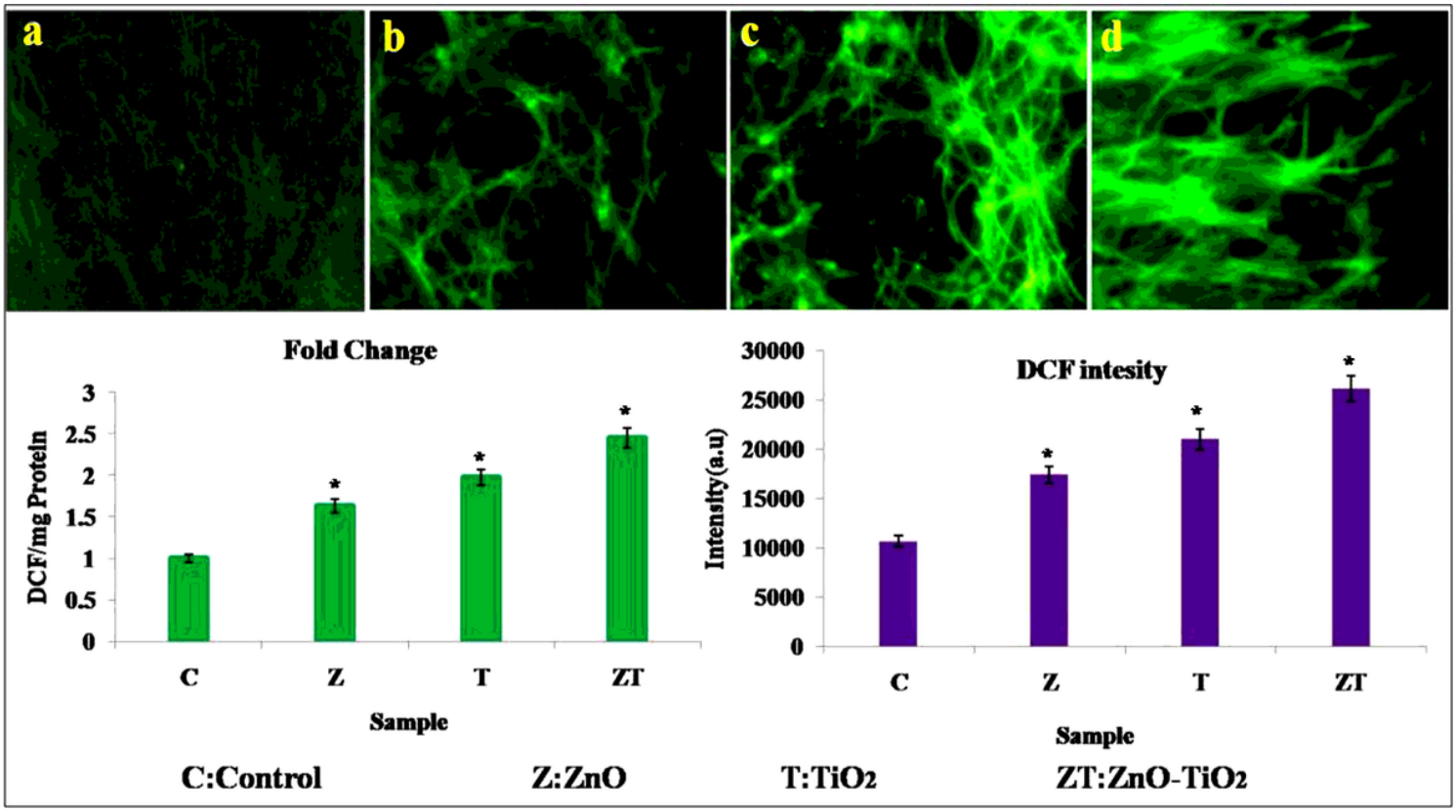

Figure 7

ROS detection of nanostructures by DCFH-DA methodology. Panels a) untreated control, b) ZnO, c) TiO2, and d) ZnO-TiO2 treated A. flavus

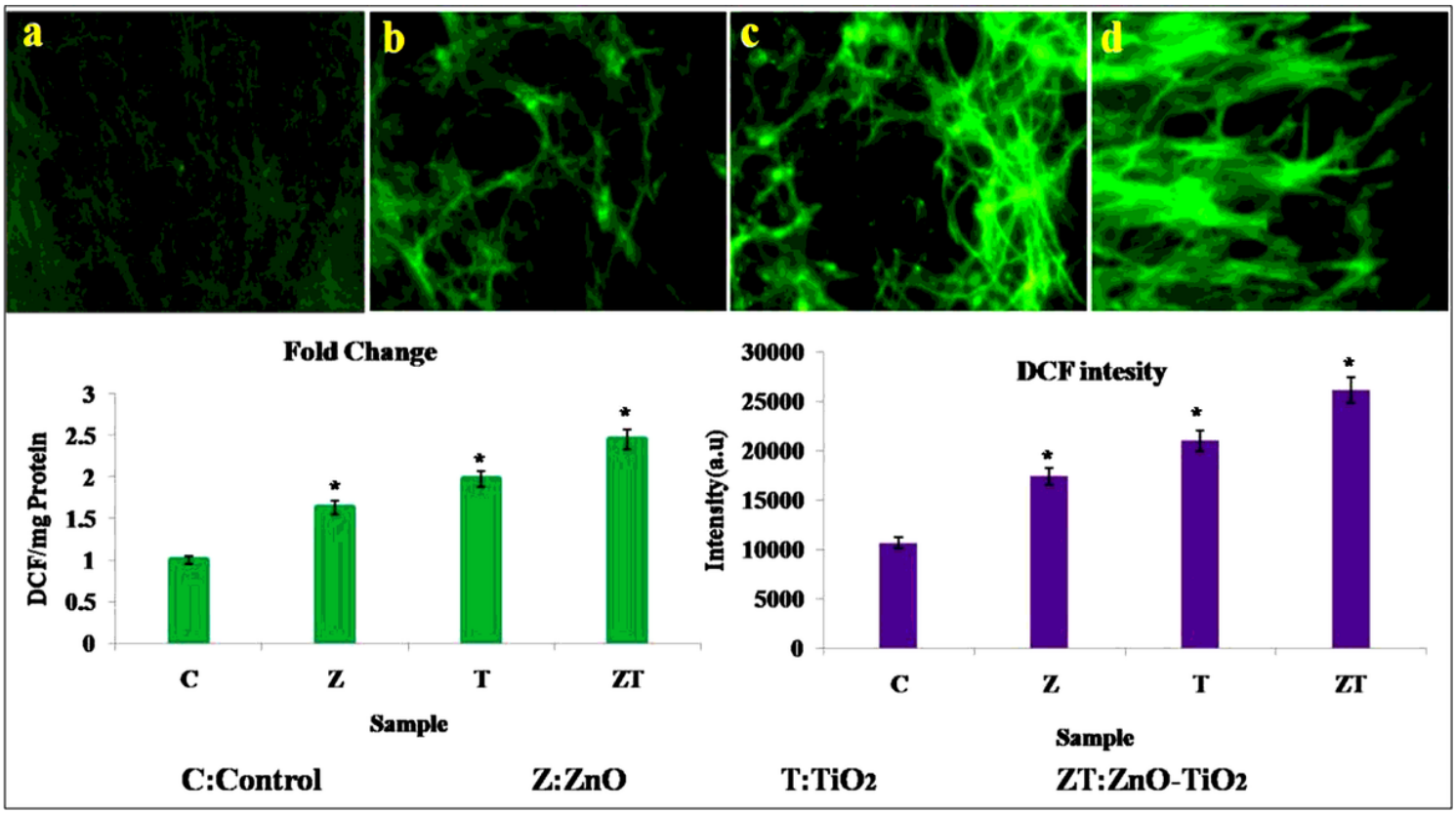

Figure 7

ROS detection of nanostructures by DCFH-DA methodology. Panels a) untreated control, b) ZnO, c) TiO2, and d) ZnO-TiO2 treated A. flavus